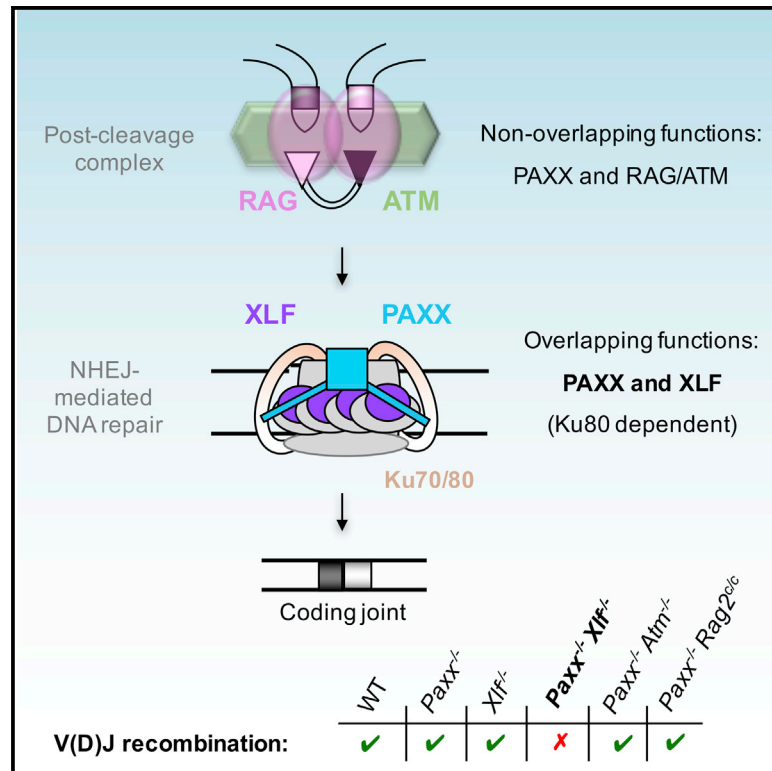


Specific Roles of XRCC4 Paralogs PAXX and XLF during V(D)J Recombination

Graphical Abstract



Authors

Chloé Lescale, H el ene Lenden Hasse, Andrew N. Blackford, ..., Bernardo Reina-San-Martin, Stephen P. Jackson, Ludovic Deriano

Correspondence

ludovic.deriano@pasteur.fr

In Brief

Developing lymphocytes rely on nonhomologous end joining (NHEJ) to repair programmed DNA double-strand breaks generated during antigen receptor gene assembly. Lescale et al. show that PAXX—a component of the NHEJ machinery—has a key role in V(D)J recombination that is masked by functional redundancy with its paralog XLF.

Highlights

- PAXX-deficient pro-B cells support normal V(D)J recombination
- PAXX and XLF are mutually redundant in repairing RAG-DNA breaks
- PAXX function in V(D)J recombination depends on its interaction with Ku
- Unlike XLF, PAXX is not redundant with ATM and the RAG complex in repairing DNA breaks



Specific Roles of XRCC4 Paralogs PAXX and XLF during V(D)J Recombination

Chloé Lescale,^{1,8} H  l  ne Lenden Hasse,^{1,8} Andrew N. Blackford,^{2,3,4} Gabriel Balmus,^{4,5} Joy J. Bianchi,^{1,6} Wei Yu,¹ L  a Bacoccina,¹ Ang  lique Jarade,¹ Christophe Clouin,¹ Rohan Sivapalan,⁴ Bernardo Reina-San-Martin,⁷ Stephen P. Jackson,^{4,5} and Ludovic Deriano^{1,9,*}

¹Departments of Immunology and Genomes and Genetics, Institut Pasteur, 75015 Paris, France

²Weatherall Institute of Molecular Medicine, University of Oxford, John Radcliffe Hospital, Oxford OX3 9DS, UK

³CRUK/MRC Oxford Institute for Radiation Oncology, Department of Oncology, University of Oxford, Oxford OX3 7DQ, UK

⁴The Wellcome Trust and Cancer Research UK Gurdon Institute, University of Cambridge, Cambridge CB2 1QN, UK

⁵Maintenance of Genome Stability, Genome Campus, Wellcome Trust Sanger Institute, Cambridge CB10 1SA, UK

⁶Cellule Pasteur, University of Paris Ren   Descartes, Sorbonne Paris Cit  , Paris 75015, France

⁷Institut de G  n  tique et de Biologie Mol  culaire et Cellulaire, INSERM-U964, CNRS-UMR7104, University of Strasbourg, 67400 Illkirch, France

⁸Co-first author

⁹Lead Contact

*Correspondence: ludovic.deriano@pasteur.fr
<http://dx.doi.org/10.1016/j.celrep.2016.08.069>

SUMMARY

Paralog of XRCC4 and XLF (PAXX) is a member of the XRCC4 superfamily and plays a role in nonhomologous end-joining (NHEJ), a DNA repair pathway critical for lymphocyte antigen receptor gene assembly. Here, we find that the functions of PAXX and XLF in V(D)J recombination are masked by redundant joining activities. Thus, combined PAXX and XLF deficiency leads to an inability to join RAG-cleaved DNA ends. Additionally, we demonstrate that PAXX function in V(D)J recombination depends on its interaction with Ku. Importantly, we show that, unlike XLF, the role of PAXX during the repair of DNA breaks does not overlap with ATM and the RAG complex. Our findings illuminate the role of PAXX in V(D)J recombination and support a model in which PAXX and XLF function during NHEJ repair of DNA breaks, whereas XLF, the RAG complex, and the ATM-dependent DNA damage response promote end joining by stabilizing DNA ends.

INTRODUCTION

V(D)J recombination assembles immunoglobulin and T cell receptor variable exons from variable (V), diversity (D), and joining (J) gene segments via a cut-and-paste mechanism (Bassing et al., 2002). This process occurs in developing lymphocytes during the G1 phase of the cell cycle and is initiated when the recombination-activating gene products RAG1 and RAG2 (forming the RAG endonuclease) introduce double-strand breaks (DSBs) among V, D, and J coding gene segments and flanking recombination signal sequences (RSSs) (Schatz and Swanson, 2011). RAG-mediated cleavage at a pair of RSSs generates

four broken DNA ends: two blunt 5' phosphorylated signal ends (SEs) that terminate in the RSS and two covalently sealed (hairpin) coding ends (CEs). After cleavage, the RAG proteins stay associated with the DNA ends in a post-cleavage complex (PCC) that is thought to contribute to end-stabilization and end-joining activities (Deriano and Roth, 2013; Schatz and Swanson, 2011). Subsequently, the classical nonhomologous end-joining (NHEJ) pathway joins these DNA ends in a recombinant configuration, forming a coding joint (CJ) (the rearranged antigen receptor gene) and a reciprocal signal joint (SJ) (Deriano and Roth, 2013; Helmink and Sleckman, 2012; Schatz and Swanson, 2011). Additionally, RAG-induced DNA breaks activate the ataxia telangiectasia mutated (ATM)-kinase-dependent DNA damage response (DDR) (Helmink and Sleckman, 2012). ATM, beyond activating p53-dependent G1/S checkpoints, contributes to the repair of chromosomal DSBs by stabilizing coding ends in post-cleavage repair complexes most likely through the activation of downstream targets (Bredemeyer et al., 2006). Thus, the stabilization and tethering of broken DNA ends depends on ATM kinase activity and the formation of ATM-dependent DNA repair foci (Helmink and Sleckman, 2012; Kumar et al., 2014).

During NHEJ, the Ku70/80 heterodimer (Ku) binds DNA ends and recruits the DNA-dependent protein kinase catalytic subunit (DNA-PKcs) in order to form the DNA-PK holoenzyme (Gottlieb and Jackson, 1993). DNA-PK phosphorylates multiple substrates, promoting synapsis of DNA ends and facilitating the recruitment of end processing and ligation enzymes. Finally, the XRCC4-Ligase 4 complex performs ligation of DNA ends (Deriano and Roth, 2013; Lieber, 2010). Deficiency for these core NHEJ factors results in severe combined immunodeficiency due to the inability to complete repair of RAG DNA breaks (Blunt et al., 1995; Deriano and Roth, 2013; Helmink and Sleckman, 2012; Revy et al., 2005; Rooney et al., 2004), thus highlighting the importance of identifying all players in this process and deciphering their functions.



XRCC4 and the XRCC4-like factor (XLF) are two members of the same protein family and share structural similarity (Andres et al., 2007; Callebaut et al., 2006; Li et al., 2008b). XLF stimulates the XRCC4/Ligase 4 complex through an uncertain mechanism, and together, XLF and XRCC4 form long filaments thought to help DNA end tethering during NHEJ (Hammel et al., 2011; Mahaney et al., 2013; Reid et al., 2015; Riballo et al., 2009; Ropars et al., 2011; Roy et al., 2015; Tsai et al., 2007). In contrast to other NHEJ factor deficiencies, XLF-deficient mice are not markedly immune-deficient, and pro-B cell lines derived from these animals perform nearly normal V(D)J recombination (Lescale and Deriano, 2016; Li et al., 2008a; Vera et al., 2013). This apparently nonessential role is at least partly due to functional redundancy between XLF and members of the ATM DDR (Kumar et al., 2014; Zha et al., 2011). Additionally, we recently demonstrated that XLF function in the repair of RAG DNA breaks is also masked by redundancy with RAG2 (Lescale et al., 2016). Consistent with this, induction of RAG-mediated recombination in pro-B cell lines deficient for XLF and ATM or expressing a C-terminal truncated form of RAG2 in the absence of XLF similarly leads to a block in V(D)J recombination and severe immune-deficiency due to an inability to repair DSB intermediates (Kumar et al., 2014; Lescale et al., 2016; Zha et al., 2011).

PAXX, a paralog of XRCC4 and XLF (Ochi et al., 2015), is a recently identified component of the NHEJ machinery (Craxton et al., 2015; Ochi et al., 2015; Xing et al., 2015). It has been shown to accumulate at sites of DNA damage and function with XRCC4 and XLF to mediate DSB repair and cell survival in response to DSB-inducing agents. PAXX itself does not bind DNA but interacts with Ku and Ku-bound DNA in order to promote NHEJ factor assembly and enhance DNA end ligation (Ochi et al., 2015; Roy et al., 2015; Xing et al., 2015). In addition, episomal recombination assays performed in HEK293 cells showed that loss of PAXX accentuates the requirement for XLF in joining coding and signal ends (Roy et al., 2015), indicating that PAXX might play important functions during antigen receptor gene assembly in lymphocytes. Here, we used a physiological RAG-inducible B cell line system to investigate the role of PAXX during V(D)J recombination and uncover potential functional interactions with XLF, the ATM-dependent DDR and the RAG complex during repair of RAG-generated DSB intermediates.

RESULTS

Generation of PAXX-Deficient *v-abl* pro-B Cells using CRISPR/Cas9 Gene Editing

We employed CRISPR/Cas9-mediated gene editing to delete *Paxx* (Δ exons1–4) from wild-type (WT) *v-Abelson* (*v-abl*) immortalized pro-B cells (Lescale et al., 2016), generating *Paxx*^{-/-} *v-abl* pro-B cell clones (Figures 1A and S1A; Table S1). *Paxx*-deleted clones were selected on the basis of PCR analysis (Figures 1B and S1B) and complete loss of PAXX protein expression (Figures 1C and S1C). In addition, we generated *Xlf*^{-/-} and *Paxx*^{-/-} *Xlf*^{-/-} *v-abl* pro-B cell clones by deleting *Xlf* (Δ exon1) from wild-type and *Paxx*^{-/-} cells (Figure S1A; Table S1; data not shown), respectively. We also generated *Xrcc4*^{-/-} clones by deleting exon3 of *Xrcc4*, which encodes part of the XRCC4 functional core region (Gao et al., 1998; Mizuta et al., 1997), from wild-

type *v-abl* pro-B cells (Figure S1A; Table S1; data not shown). To test whether PAXX-deficient *v-abl* pro-B cells harbor defects in NHEJ-mediated DSB repair, we performed survival assays after exposing the cells to ionizing radiation. We found that *Paxx*^{-/-} *v-abl* pro-B cell clones were significantly more radiosensitive than wild-type *v-abl* pro-B cell lines but less sensitive than XLF- and XRCC4-deficient *v-abl* pro-B cells (Figure 1D; Table S2). Strikingly, the loss of both PAXX and XLF in *Paxx*^{-/-} *Xlf*^{-/-} pro-B cells led to extreme radiosensitivity in comparison to WT, PAXX, XLF, and XRCC4 single-mutant cells. Thus, we find that PAXX and XLF are not epistatic for the repair of irradiation-induced DNA damage in mouse *v-abl* pro-B cells.

Igk Rearrangement in PAXX- and PAXX/XLF-Deficient pro-B Cells

Treatment of *v-abl* immortalized pro-B cells with a *v-abl* kinase inhibitor (STI571, hereafter referred to as ABLki) leads to G1 cell-cycle arrest, the rapid induction and stabilization of RAG1/2 gene expression, and rearrangement of the endogenous *Igk* locus or any introduced V(D)J recombination reporter substrate (Bredemeyer et al., 2006; Lescale et al., 2016; Muljo and Schliessel, 2003). To elucidate whether PAXX has a role in RAG-mediated DSB repair in lymphocytes, we initially quantified the presence of DNA-damage-associated protein (53BP1) foci at the *Igk* locus in G1-arrested pro-B cells using automated 3D microscopy (Lescale et al., 2016). As expected (Lescale et al., 2016), upon treatment with ABLki for 3 days, we found that 31.1% of WT pro-B cells showed intense 53BP1 foci, the majority of which contained a single distinct spot, although cells were occasionally found to contain two, and less frequently three or more, foci (Figures 2A and 2B; Table S3). In ABLki-treated RAG2-deficient pro-B cells (*Rag2*^{-/-}), 53BP1 foci were detected in only 18.2% of the cells, consistent with the absence of RAG cleavage in these cells (Lescale et al., 2016; Shinkai et al., 1992). The few foci observed in the absence of RAG activity likely result from incomplete DNA synthesis during S phase leading to the DDR and formation of 53BP1 domains during subsequent G1 (Harrigan et al., 2011). Interestingly, 43% of PAXX-deficient pro-B cells showed 53BP1 foci, slightly more than in WT pro-B cells and comparable to XLF-deficient cells (46.6%). However, strikingly, we found that 80.1% of *Paxx*^{-/-} *Xlf*^{-/-} pro-B cells harbored 53BP1 foci similar to Ku80 (64.5%) and XRCC4 (73.5%) deficiency (Figures 2A and 2B; Table S3). Also reminiscent of Ku80- and XRCC4-deficient pro-B cells, 20.1% of *Paxx*^{-/-} *Xlf*^{-/-} cells contained two 53BP1 foci corresponding to DNA breaks at both *Igk* alleles (Lescale et al., 2016) in comparison to 3.6%, 4.3%, 6.1%, and 7.3% in *Rag2*^{-/-}, WT, *Paxx*^{-/-}, and *Xlf*^{-/-} pro-B cells, respectively (Figures 2A and 2B; Table S3). These results indicate that RAG-mediated DNA breaks are readily formed in PAXX- and PAXX/XLF-deficient cells, however, and in contrast to single deficiency, repair of these DNA breaks does not seem to occur in combined PAXX/XLF deficient cells, paralleling what is seen in the absence of the canonical NHEJ factors Ku80 and XRCC4.

Consistent with the accumulation of 53BP1 foci in *Paxx*^{-/-} *Xlf*^{-/-} pro-B cells, PCR amplification of inversional *IgkV₆₋₂₃-J₁* rearrangement (Figure 2C) in these cells revealed an almost complete lack of CJ formation, validating the presence of a

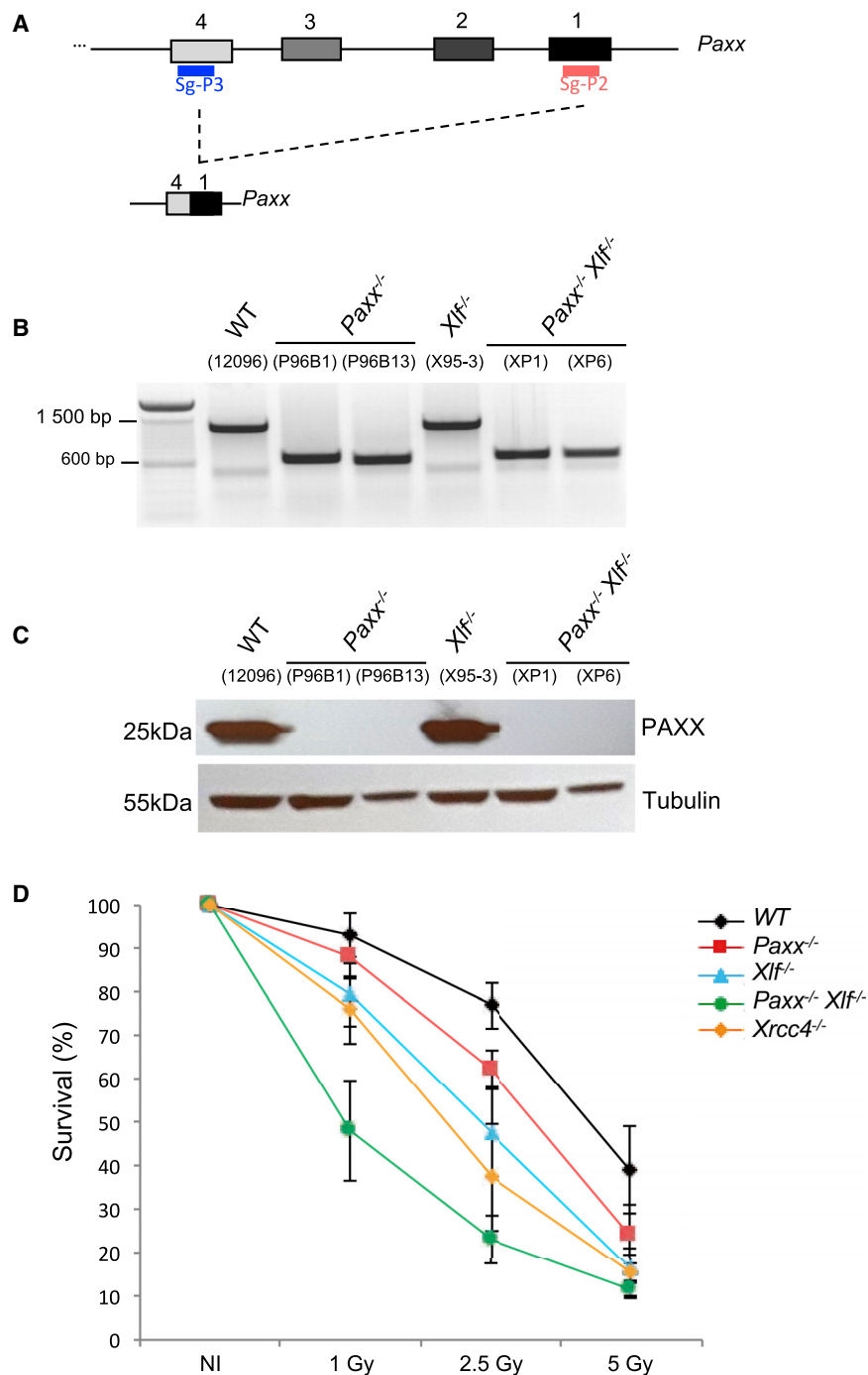


Figure 1. CRISPR/Cas9-Mediated Deletion of Paxx in *v-abl* pro-B Cells and Irradiation Sensitivity

(A) CRISPR/Cas9 *Paxx* knockout strategy. Exons are shown in boxes, and sgRNA positions are indicated. See also Figure S1A.

(B) PCR analysis showing the deletion of approximately 626 bp in the *Paxx* gene (WT = 1,299 bp band; *Paxx* KO ≈ 673 bp band). See also Figure S1B.

(C) Western blot showing the absence of the PAXX protein in *Paxx*-deleted pro B cell clones. See also Figure S1C.

(D) Irradiation sensitivity of *v-abl* pro-B cell lines. The graph represents mean ± SEM of three independent experiments using two independent cell lines (see also Table S2). Numbers indicate the percentage of survival 3 days after irradiation at 1, 2.5, and 5 Gy. See also Table S2.

from the aberrant joining of a coding to a signal end, in *Atm*^{-/-} and *Xlf*^{-/-} cells, consistent with a role for ATM and XLF in stabilizing cleaved DNA ends and thus suppressing HJs (Bredemeyer et al., 2006; Lescale et al., 2016). In contrast, analysis of *IgkV*₆₋₂₃-*J*₁ rearrangements in PAXX-deficient pro-B cells did not reveal HJs, suggesting that PAXX, unlike its paralog XLF, most likely has a very minor, if any, role in stabilizing DNA ends within post-cleavage complexes (Figure 2D, see also below and Discussion).

Coding and Signal Joint Defects in *Paxx*^{-/-} *Xlf*^{-/-} pro-B Cells

To unequivocally test for V(D)J recombination defects in PAXX/XLF-deficient cells, we transduced *v-abl* pro-B cell lines from each genotype with the pMX-RSS-GFP/IRES-hCD4 retroviral recombination substrate (pMX-INV) in which GFP is expressed upon successful chromosomal inversive RAG-mediated recombination and allows for the assessment of the rearrangement status and recombination intermediates by Southern blot analysis (Figure 3A) (Bredemeyer et al., 2006; Lescale et al., 2016). Both assays

specific end-joining defect in the absence of functional PAXX and XLF during V(D)J recombination (Figure 2D). Induction of RAG in WT, *Xlf*^{-/-}, and *Paxx*^{-/-} pro-B cells triggered robust *Vk*-to-*Jk* inversive CJ formation, whereas there was a complete absence of *IgkV*₆₋₂₃-*J*₁ rearrangements after the induction of RAG in *Xrcc4*^{-/-} pro-B cells due to the function of XRCC4 in repairing RAG-DSBs (Li et al., 1995). Notably, nested PCR amplification of inversive *IgkV*₆₋₂₃-*J*₁ rearrangement also revealed the formation of deletional hybrid joints (HJs), which results

confirmed robust levels of rearrangements in ABLki-treated WT, *Xlf*^{-/-}, and *Paxx*^{-/-} cells (Figures 3B and 3C). Interestingly, although both *Paxx*^{-/-} and *Xlf*^{-/-} pro-B cells are proficient at recombining, we consistently found significantly higher levels of rearrangements in *Paxx*^{-/-} pro-B cells than *Xlf*^{-/-} pro-B cells (Figure 3B, 45% recombination in *Paxx*^{-/-} cells versus 26% recombination in *Xlf*^{-/-} cells, *p* < 0.001, Figure 3C). These results are reminiscent of the stronger radiation sensitivity observed in XLF-deficient cells in comparison to PAXX-deficient cells

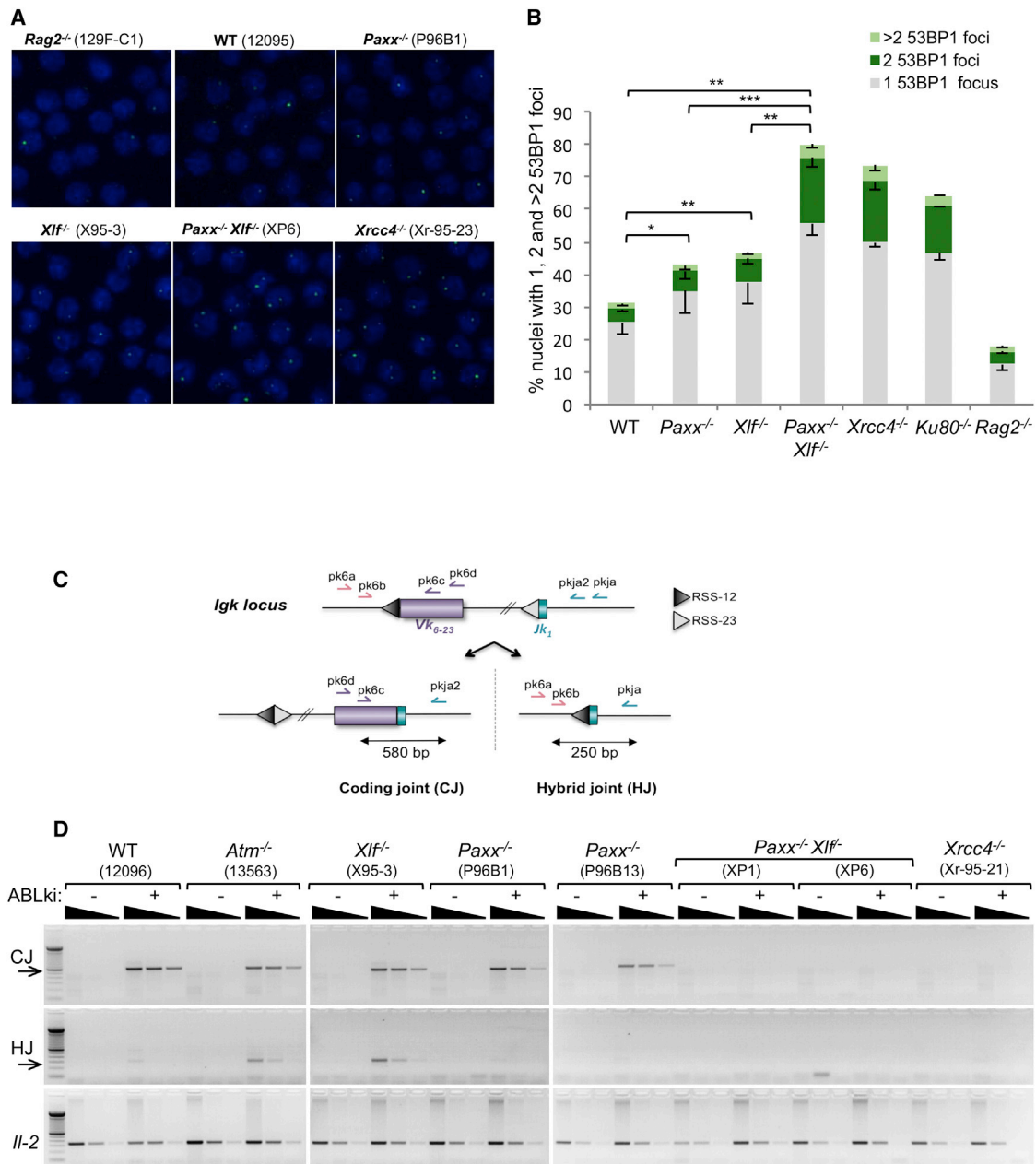


Figure 2. Accumulation of 53BP1 DDR Foci and Impaired *Igk* Rearrangement in *Paxx*^{-/-} *Xlf*^{-/-} pro-B Cells

(A) Representative 3D projections of 53BP1 immunostaining conducted on ABLki-treated *v-abl* pro-B cells.

(B) Percentage of *v-abl* pro-B cells harboring 1, 2, or >2 53BP1 foci 65 hr post ABLki treatment. Data represent mean ± SEM from three independent experiments with one or two independent cell lines for each genotype. See also Table S3.

(C) Schematic of the *Igk* locus with position of primers (arrows) used to assay coding joint (CJ) and hybrid joint (HJ) formation during inversional *IgkV₆₋₂₃-J₁* rearrangement.

(D) Semiquantitative nested PCR analysis of *IgkV₆₋₂₃-J₁* coding joints (CJ) and hybrid joints (HJ) from indicated *v-abl* pro-B cell lines treated for 72h with ABLki. *Il-2* gene PCR was used as a loading control.

(Figure 1D) and suggest that XLF deficiency leads to a more profound defect in repairing DSB than PAXX deficiency.

Strikingly, flow cytometry analysis revealed severely impaired inversional rearrangement in *Paxx*^{-/-} *Xlf*^{-/-} cells in comparison to WT (≈115-fold decrease, *p* < 0.001), *Paxx*^{-/-} (≈97-fold

decrease, *p* < 0.001), and *Xlf*^{-/-} (≈56-fold decrease, *p* < 0.001) cells (Figure 3B). Southern blot and PCR analysis confirmed severe end-joining defects in *Paxx*^{-/-} *Xlf*^{-/-} cells, as revealed by a marked decrease in CJs and a marked increase in unjoined CE, indicative of a classical NHEJ defect (Figures

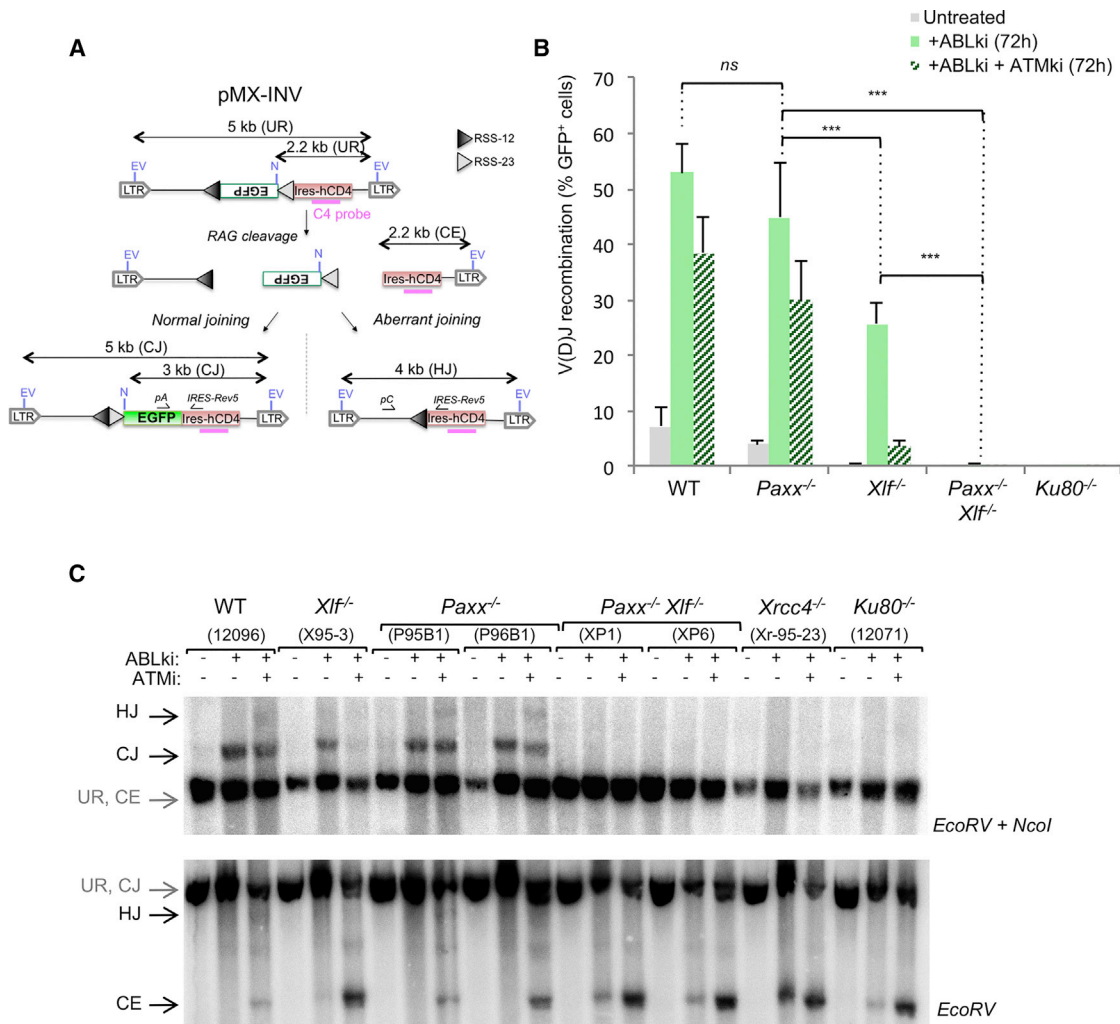


Figure 3. Defective Inversional V(D)J Recombination in *Paxx*^{-/-} *Xlf*^{-/-} B Cells

(A) Schematic of pMX-INV recombination substrate. The 12 recombination signal sequence (RSS-12; black triangle), GFP cDNA, 23 recombination signal sequence (RSS-23; gray triangle), internal ribosome entry site (IRES)-human CD4 cDNA (IRES-hCD4), long-terminal repeats (LTRs), EcoRV (EV) sites, NcoI (N) site, C4 probe (pink bar), and the expected sizes for the un-rearranged substrate (UR), coding end intermediates (CE), CJs and HJs are indicated.

(B) *v-abl* pro-B cell lines treated for 72 hr with ABLki with or without ATM kinase inhibitor (ATMki) were assayed for pMX-INV rearrangement by flow cytometry with the percentage of GFP expressing cells indicated. Data represent mean ± SEM of at least four independent experiments using two WT (12095 and 12096), two *Paxx*^{-/-} (P96B1 and P96B13), four *Xlf*^{-/-} (16218, 16488, X95-3, and X95-4), two *Paxx*^{-/-} *Xlf*^{-/-} (XP1 and XP6), and one *Ku80*^{-/-} (12071) independent cell lines. *, 0.01 ≤ *p* < 0.05; **, 0.001 ≤ *p* < 0.01; ***, *p* < 0.001.

(C) The indicated *v-abl* pro-B cell lines containing the pMX-INV substrate were treated for 72 hr with ABLki with or without ATMki and assayed by Southern blotting with EcoRV/NcoI digest-C4 probe (top) and EcoRV digest-C4 probe (bottom). See also Figure S2.

3C and S2). Notably, the intensity of the inversional V(D)J recombination defect in *Paxx*^{-/-} *Xlf*^{-/-} cells was similar to that of *Ku80*^{-/-} and *XRCC4*-deficient cells (Figures 3B and 3C). *Paxx*^{-/-} *Xlf*^{-/-} cells treated with ABLki and the ATM-specific inhibitor *Ku55933* (ATMki) (Hickson et al., 2004) showed stronger levels of unrepaired CEs in comparison to ABLki-treated *Paxx*^{-/-} *Xlf*^{-/-} cells, indicating that a fraction of unrepaired CEs are subjected to ATM-dependent end degradation in *PAXX*/*XLF*-deficient cells similar to what has been previously reported in the context of *Ku80*, core *RAG2*/*XLF*, *H2AX*/*XLF*, and *53BP1*/*XLF* deficiency (Helmink et al., 2011; Lescale and Deriano, 2016; Zha et al., 2011).

To identify specific defects in CJ and SJ formation, we generated multiple *v-abl* pro-B cell lines from each genotype that harbored either a chromosomal deletional substrate designed to assay CJs and unjoined CEs (pMX-DEL^{CJ}; Figure 4A) or a chromosomal deletional substrate designed to assay SJs and unjoined SEs (pMX-DEL^{SJ}; Figure 4B) (Bredemeyer et al., 2006). In agreement with the aforementioned observations, induction of RAG in WT, *Xlf*^{-/-}, and *Paxx*^{-/-} cells generated substantial CJ and SJ levels with no obvious free CEs and SEs (Figures 4C, 4D, and S3). By contrast, *Paxx*^{-/-} *Xlf*^{-/-} cells had very little accumulation of CJs or SJs, which were only detectable after PCR amplification, and, instead accumulated un-joined CEs

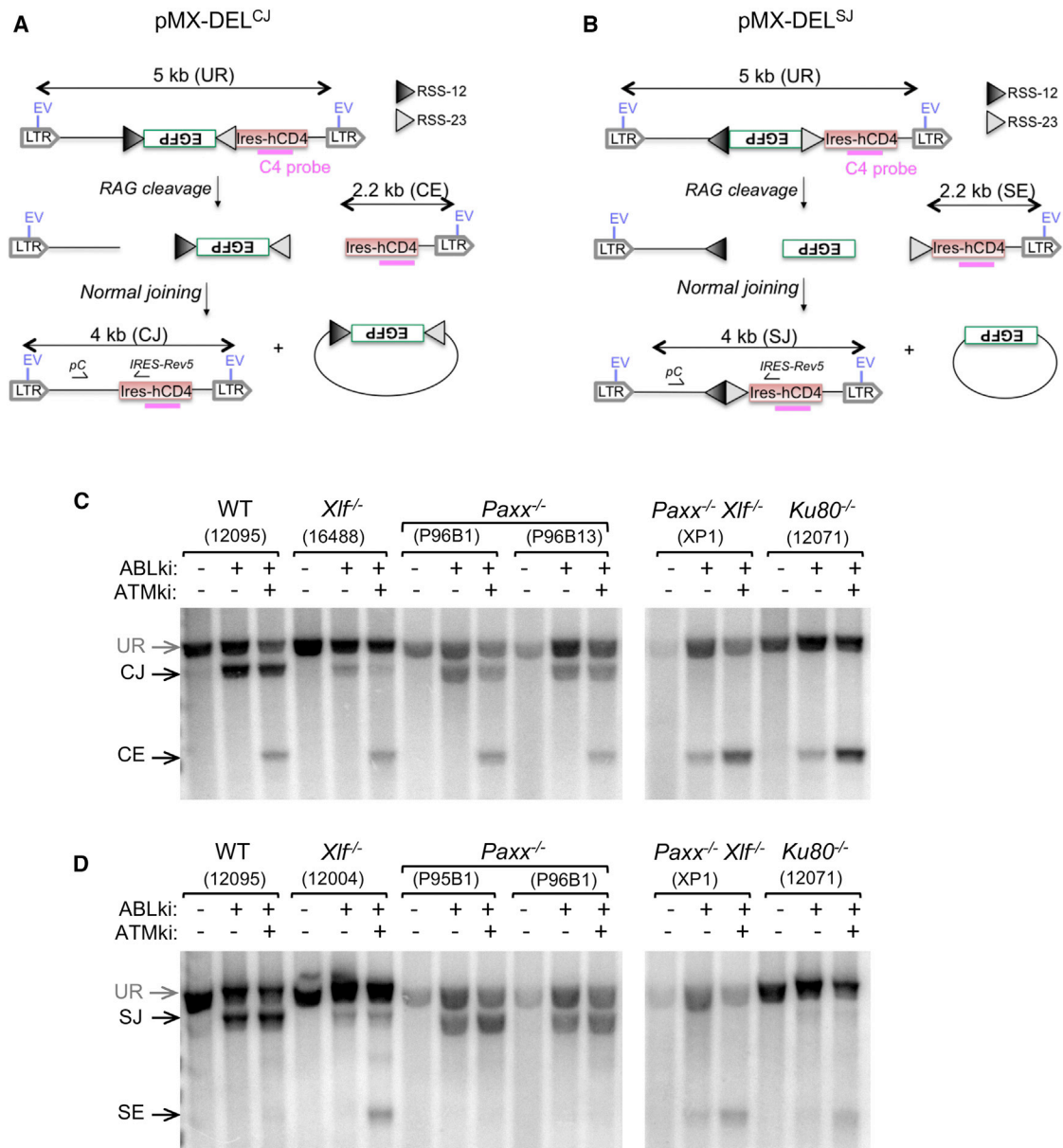


Figure 4. Defective Deletional V(D)J Recombination in Paxx^{-/-} Xlf^{-/-} B Cells

(A and B) Schematics of pMX-DEL^{CJ} (A) and pMX-DEL^{SJ} (B) recombination substrates with intermediates and products as defined for pMX-INV (Figure 3A). (C and D) *v-abl* pro-B cell lines containing pMX-DEL^{CJ} (C) or pMX-DEL^{SJ} (D) were treated for 72 hr with ABLki with or without ATMki and assayed by Southern blotting with EcoRV digest-C4 probe. See also Figures S3 and S4 and Table S4.

and SEs (Figures 4C and 4D and S3). To determine the fidelity of rare SJ formation in Paxx^{-/-} Xlf^{-/-} cells, we subjected SJ PCR products to digestion with the restriction enzyme *Apa*I, which exclusively digests SJs formed without the loss or addition of nucleotides (Bogue et al., 1998; Ramsden et al., 1997). Unlike SJs formed in WT and PAXX-deficient pro-B cells, which are largely *Apa*I sensitive, SJs derived from PAXX/XLF- and Ku80-deficient pro-B cells were almost exclusively resistant to *Apa*I digestion, indicating that the rare SJs formed in these cells were imperfect (Figure S4A). SJs from XLF-deficient pro-B cells were also imper-

fect, although to a lesser extent than those observed in Paxx^{-/-} Xlf^{-/-} and Ku80^{-/-} cells (Figure S4). Consistently, sequencing of SJs derived from Paxx^{-/-} Xlf^{-/-} and Ku80^{-/-} cells revealed increased deletions and utilization of micro-homology in comparison to WT, Paxx^{-/-}, and Xlf^{-/-} cells (Figures S4B–S4D; Table S4), demonstrating aberrant joining of signal ends by alternative NHEJ (Deriano and Roth, 2013) in PAXX/XLF-deficient pro-B cells. Taken together, these results provide strong evidence that PAXX and XLF double deficiency leads to a severe NHEJ defect in recombining lymphocytes.

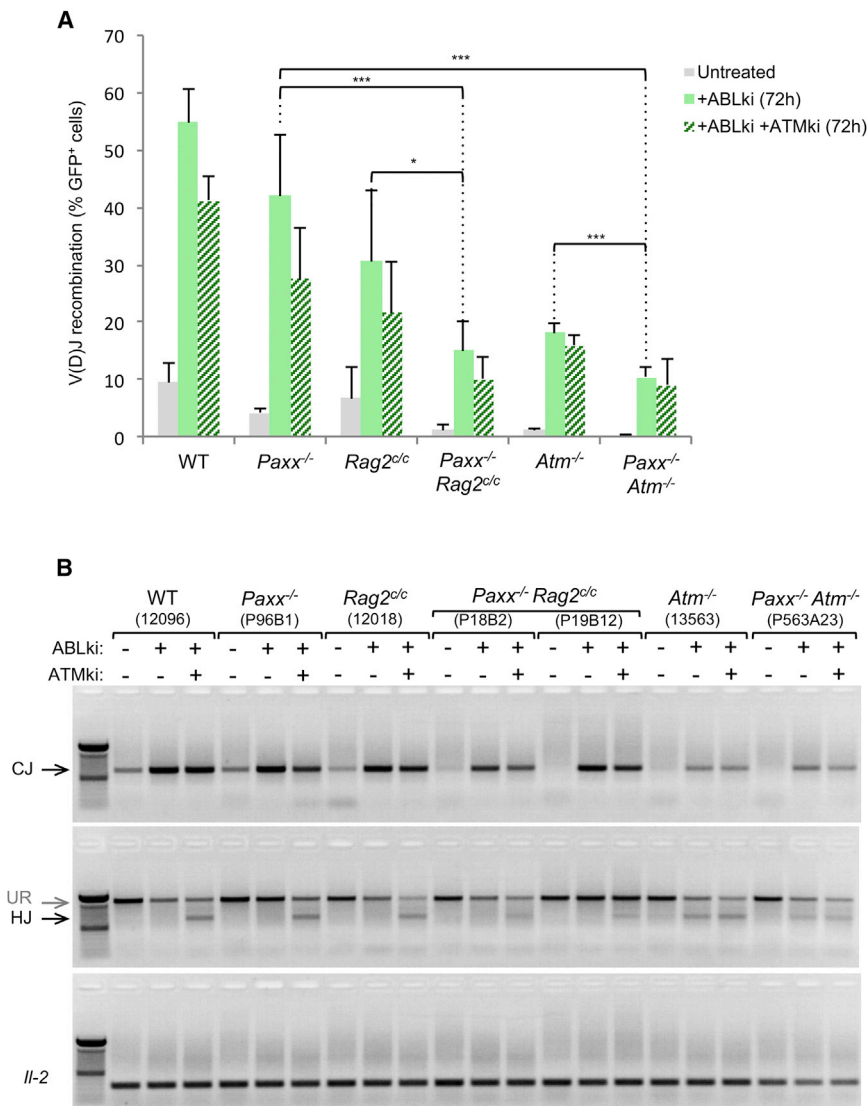


Figure 5. *Paxx*^{-/-} *Atm*^{-/-} and *Paxx*^{-/-} *Rag2*^{c/c} B Cells Perform Robust V(D)J Recombination

(A) *v-abl* pro-B cell lines treated for 72 hr with ABLki with or without ATM kinase inhibitor (ATMki) were assayed for pMX-INV rearrangement by flow cytometry with the percentage of GFP expressing cells indicated. Data represent mean \pm SEM of at least four independent experiments with two WT (12095 and 12096), two *Paxx*^{-/-} (P96B1 and P96B13), two *Rag2*^{c/c} (12018 and 12019), two *Paxx*^{-/-} *Rag2*^{c/c} (P18B2 and P19B12), two *Atm*^{-/-} (160 and 13563), and one *Paxx*^{-/-} *Atm*^{-/-} (P563A23) independent cell lines. *, 0.01 \leq p < 0.05; **, 0.001 \leq p < 0.01; ***, p < 0.001.

(B) PCR analysis of pMX-INV CJs and HJs from indicated *v-abl* *abl* pro-B cell lines treated for 72 hr with ABLki with or without ATMki. *Il-2* gene PCR was used as a loading control.

decrease in the percentage of GFP-positive pro-B cells (Figure 3B) and the accumulation of CEs instead of CJ products (Figure 3C). Inhibition of the ATM kinase activity in WT led to robust recombination (Figure 3B) and a specific accumulation of CEs (Figures 3C, 4C, 4D, S2, and S3) due to the role of ATM in stabilizing coding ends within post-cleavage complexes (Bredemeyer et al., 2006; Helmink and Sleckman, 2012). Strikingly, and in sharp contrast to XLF deficiency, pMX-INV rearrangement was not dramatically affected in *Paxx*^{-/-} pro-B cells treated with ATMki in comparison to untreated *Paxx*^{-/-} pro-B cells and ATMki-treated WT pro-B cells (Figures 3B, 3C, and S2). Consistently, we also observed robust CJ and SJ formation in pMX-DEL^{CJ} *Paxx*^{-/-} pro-B cells and pMX-DEL^{SJ}

PAXX Function in V(D)J Recombination Does Not Overlap with ATM

Previous studies have shown that XLF functions in a cooperative manner with several members of the ATM-dependent DSB response pathway in joining DNA breaks during V(D)J recombination (Kumar et al., 2014; Zha et al., 2011). Because the ATM-DSB response relies on the kinase activity of ATM, treatment of XLF-deficient pro-B cells with an ATM-specific inhibitor abrogates V(D)J recombination in these cells (Kumar et al., 2014; Lescale et al., 2016; Zha et al., 2011). Based on the structural similarities that exist between XLF and PAXX (Ochi et al., 2015; Xing et al., 2015), we envisioned that PAXX might also be functionally redundant with the ATM-DSB response during V(D)J recombination. To test this hypothesis, we treated pMX-INV-transduced *v-abl* pro-B cell lines with ABLki and ATMki (Figures 3 and S2). As expected (Lescale et al., 2016; Zha et al., 2011), rearrangement was almost completely abolished in *Xlf*^{-/-} pro-B cells treated with ATMki, leading to a strong

Paxx^{-/-} pro-B cells treated with ATMki, respectively (Figures 4C, 4D, and S3). Altogether, these results indicate that PAXX does not rely on ATM kinase activity during V(D)J recombination.

To further substantiate that PAXX function in V(D)J recombination is not redundant with ATM, we also generated PAXX/ATM doubly deficient pro-B cell lines by deleting *Paxx* from *Atm*^{-/-} pro-B cells (Figure S1; Table S1; data not shown). To quantify V(D)J recombination efficiency, we chromosomally integrated the pMX-INV substrate in pro-B cell clones (Figure 3A) and triggered RAG expression. In contrast to *Xlf*^{-/-} *Atm*^{-/-} pro-B cells (Zha et al., 2011) and *Paxx*^{-/-} *Xlf*^{-/-} pro-B cells (Figure 3B) and in agreement with our ATMki results (Figures 3 and 4), PAXX/ATM double knockout pro-B cells performed quite robust inversions recombination in comparison to ATM single knockout pro-B cells (Figures 5A and 5B). These results indicate that, although XLF and PAXX paralogs functionally overlap in repairing RAG-induced signal ends and coding ends, they diverge with regard to their respective redundancy with ATM.

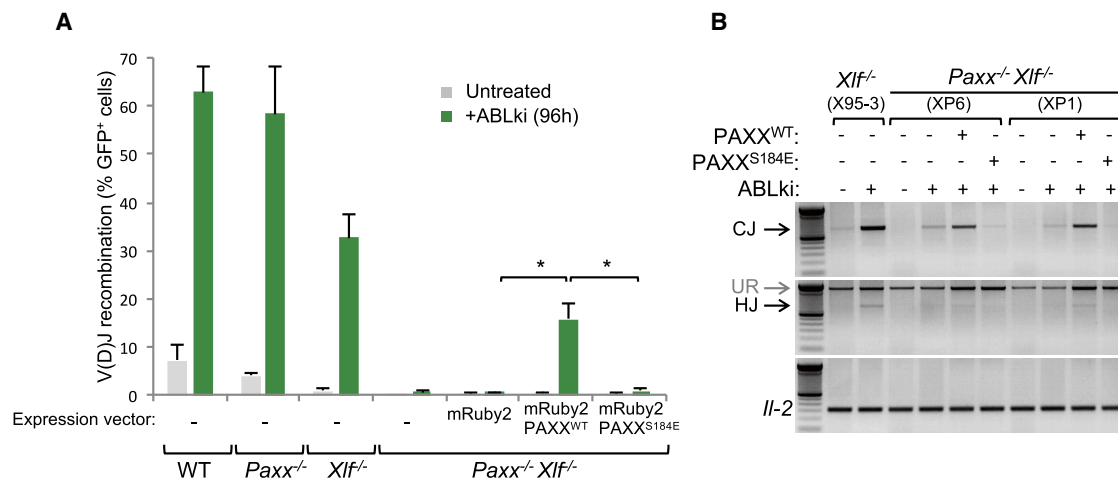


Figure 6. PAXX Function in the Absence of XLF Depends on Its Interaction with Ku

(A) *Paxx*^{-/-} *Xlf*^{-/-} *v-abl* pro-B cell lines (XP1, XP6) were transfected with expression vectors encoding for mRuby2, mRuby2-PAXX^{WT}, or mRuby2-PAXX^{S184E}. After 6 hr recovery, *Paxx*^{-/-} *Xlf*^{-/-} transfected cells, along with controls, were treated for 96 hr with ABLki and assayed for pMX-INV rearrangement by flow cytometry with the percentage of GFP-expressing cells indicated. Data represent mean ± SEM of three independent experiments using two independent cell lines for each genotype. See also Figure S6.

(B) PCR analysis of pMX-INV CJs and HJs from control and ABLki-treated *Xlf*^{-/-} and *Paxx*^{-/-} *Xlf*^{-/-} pro-B cell lines expressing mRuby2-PAXX^{WT} or mRuby2-PAXX^{S184E}. *Il-2* gene PCR was used as a loading control.

PAXX Function in V(D)J Recombination Does Not Overlap with the RAG2 C Terminus

We recently showed that XLF also cooperates with the RAG complex in repairing DNA breaks. Thus, in the context of RAG2 lacking the C terminus domain (*Rag2*^{c/c} mutant, also referred to as core RAG2), XLF deficiency leads to a profound lymphopenia associated with a severe defect in V(D)J recombination (Lescale et al., 2016). These results led us to propose a model in which the RAG proteins and the ATM-DSB response might participate in a same pathway (i.e., allowing the stabilization of cleaved DNA ends) that is functionally redundant with XLF (Lescale et al., 2016). To test for potential functional interaction between the RAG complex and PAXX, we deleted *Paxx* from core RAG2-expressing *v-abl* pro-B cell lines (Lescale et al., 2016) (Figure S1; Table S1). Induction of RAG in pMX-INV transduced *Paxx*^{-/-} *Rag2*^{c/c} pro-B cells led to robust recombination in comparison to core RAG2-expressing pro-B cells as measured by flow cytometry and PCR analysis (Figures 5A and 5B). In addition, pMX-INV rearrangement was not dramatically affected in *Paxx*^{-/-} *Rag2*^{c/c} pro-B cells treated with the ATMki in comparison to untreated *Paxx*^{-/-} *Rag2*^{c/c} pro-B cells and ATMki-treated *Rag2*^{c/c} pro-B cells (Figures 5A and 5B). Together, these results demonstrate that, unlike XLF, PAXX does not functionally overlap with the RAG complex in the repair of RAG-generated DNA ends. These findings also indicate that, during V(D)J recombination, the redundancy between XLF and PAXX is mechanistically distinct from the previously reported redundancy between XLF and RAG/ATM-DDR (Kumar et al., 2014; Lescale et al., 2016; Zha et al., 2011).

PAXX Function in the Absence of XLF Depends on Its Interaction with Ku

We recently reported that PAXX function during the repair of ionizing radiation-induced DNA damage depends on its ability

to bind Ku (Ochi et al., 2015). PAXX-Ku interaction stimulates DNA end ligation by Ligase 4, promotes assembly of core NHEJ factors on damaged chromatin, and depends on the C terminus of PAXX, specifically residues V199 and F201 (Ochi et al., 2015). Here, we found that mutating the highly conserved residue S184 to glutamate (PAXX^{S184E}) similarly abolishes PAXX interaction with Ku (Figure S5). To investigate whether the PAXX-Ku interaction is required for V(D)J recombination in the context of XLF deficiency, we expressed mRuby2 fluorescent protein (mRuby2), mRuby2-tagged WT PAXX protein (mRuby2-PAXX^{WT}), and mRuby2-PAXX^{S184E} protein in pMX-INV *Paxx*^{-/-} *Xlf*^{-/-} pro-B cells (Figure 6). Expression of mRuby2-PAXX^{WT}, but not mRuby2 and mRuby2-PAXX^{S184E}, substantially restored recombination in RAG-induced *Paxx*^{-/-} *Xlf*^{-/-} pro-B cells (Figure 6A). In line with this, complementation with PAXX^{WT} in *Paxx*^{-/-} *Xlf*^{-/-} pro-B cells also led to the formation of CJs and HJs characteristic of XLF single deficiency (Lescale et al., 2016) (Figure 6B). To strengthen these results, we transfected *Paxx*^{-/-} *Xlf*^{-/-} pro-B cells carrying a modified m-Cherry version of the pMX-INV recombination substrate (Figure S6A) with expression vectors (Ochi et al., 2015) encoding for GFP, GFP-tagged PAXX^{WT}, GFP-tagged C-terminally truncated PAXX¹⁻¹⁴⁵, and GFP-tagged PAXX^{V199A/F201A}. Ectopic expression of GFP-PAXX^{WT}, but not the Ku interaction-deficient proteins GFP-PAXX¹⁻¹⁴⁵ and GFP-PAXX^{V199A/F201A}, partially restored RAG-mediated rearrangements in *Paxx*^{-/-} *Xlf*^{-/-} pro-B cells (Figure S6B). Together, these data support a model in which the PAXX-Ku interaction is crucial for PAXX function in V(D)J recombination.

DISCUSSION

PAXX, XRCC4, and XLF comprise a homologous superfamily of structurally related proteins that participate in the repair of DSBs

by NHEJ (Ochi et al., 2015; Ochi et al., 2014). Here, we show that PAXX has a key role in V(D)J recombination that is masked by functional redundancy with XLF. Our results support a model in which the PAXX, XRCC4, and XLF paralogs play distinct redundant and nonredundant functions in the repair of RAG-generated DNA ends, specifically in the locking and joining steps, during antigen receptor gene assembly (Figure 7).

Recent studies have shown that XLF is redundant with several members of the ATM-DDR and the RAG complex in joining broken DNA ends (Deriano and Roth, 2013; Helmink and Sleckman, 2012; Kumar et al., 2014; Lescale et al., 2016; Zha et al., 2011). This redundancy is thought to rely, at least partially, on the ability of these complexes to assemble a synaptic complex that bridges DNA ends: the ATM-DDR through the formation of chromatin-associated DNA repair foci, the RAG complex through an unknown mechanism, and XLF via the formation of XLF/XRCC4 DNA end-bridging filaments. In contrast to XLF, we conclude that, based on several observations, PAXX does not participate in stabilizing RAG-DNA breaks (Figure 7). We reveal that *Paxx*^{-/-} *Atm*^{-/-} pro-B cells support robust V(D)J recombination, demonstrating that, unlike XLF, PAXX does not functionally overlap with ATM in repairing coding and signal ends (Figures 3–5, S2, and S3). Notably, we observed a small but significant decrease in overall recombination in *Paxx*^{-/-} *Atm*^{-/-} pro-B cells in comparison to *Paxx*^{-/-} pro-B cells and *Atm*^{-/-} pro-B cells (Figure 5A). This decrease could be attributed to additive NHEJ defects in the absence of PAXX and ATM (Craxton et al., 2015; Kumar et al., 2014; Ochi et al., 2015; Xing et al., 2015). We also found that, similar to PAXX/ATM deficiency, PAXX-deficient pro-B cells expressing the core RAG2 mutant protein (*Paxx*^{-/-} *Rag2*^{c/c}) perform robust V(D)J recombination. Additionally, treatment of *Paxx*^{-/-} *Rag2*^{c/c} pro-B cells with a specific ATM kinase inhibitor does not abrogate recombination in these cells (Figure 5), indicating that, in the absence of a functional RAG/ATM-DDR complex, PAXX is not required for synapsis and joining of DNA ends. In line with this, destabilization of the post-cleavage synaptic complex in *Atm*^{-/-} and *Xlf*^{-/-} pro-B cells irretrievably leads to the formation of HJs (Bredemeyer et al., 2006; Lescale et al., 2016); however, we did not detect HJs in recombining PAXX-deficient pro-B cells (Figure 2). Lastly, in line with previous results (Bredemeyer et al., 2006), we show that ATM deficiency leads to the accumulation of coding ends but not signal ends (Figure 4). This discrepancy is thought to rely on the proclivity of the RAG to bind more avidly to signal end pairs in comparison to coding end pairs (Agrawal and Schatz, 1997; Bredemeyer et al., 2006; Helmink and Sleckman, 2012; Hiom and Gellert, 1998; Schatz and Swanson, 2011). Combined ATM/XLF deficiency leads to an almost complete lack of CJs associated with an accentuated accumulation of coding ends and to the accumulation of signal ends, which is consistent with a redundant role for XLF in stabilizing DNA ends (Figure 4) (Zha et al., 2011). In sharp contrast, we find that PAXX/ATM deficiency does not affect coding and signal DSB intermediates beyond that of ATM single deficiency (Figures 4, 5, and S3). Altogether, our results strongly indicate that PAXX does not play a major role in stabilizing and tethering DNA ends during RAG-mediated rearrangements (Figure 7). Interestingly, Roy et al., (2015) have also recently shown that

PAXX does not enhance the cellular requirement for XRCC4/XLF interaction and potential DNA end bridging in human epithelial cells.

We find that, upon RAG cleavage, more than 80% of *Paxx*^{-/-} *Xlf*^{-/-} pro-B cells accumulate 53BP1 DNA damage foci (Figures 2A and 2B). This is consistent with the accumulation of unrepaired RAG-DNA ends in these cells and in the context of other end-joining deficiency such as in XRCC4-, Ku80-, and core-RAG2/XLF-deficient cells (Figures 2–4, S2, and S3) (Lescale et al., 2016). Notably, a fraction of these 53BP1 foci might also arise due to under-replicated DNA (Harrigan et al., 2011). This possibility is in agreement with the observation that fibroblasts derived from immune-deficient patients carrying XLF mutations exhibit impaired cellular response to replication stress (Schwartz et al., 2009). It will be interesting to investigate the specific roles of XRCC4 paralogs and, more generally, components of the NHEJ pathway, during replication and to determine to which extent it contributes to the formation of 53BP1 foci in G1-arrested cells. Nonetheless, the complete lack of rearrangement and accumulation of unrepaired DNA ends observed in XLF/PAXX-deficient pro-B cells is consistent with a severe end-joining defect in these cells (Figures 2–4, S2, and S3). In line with a role for PAXX in NHEJ-mediated repair, we find that PAXX-Ku interaction is required for PAXX function in V(D)J recombination in the absence of XLF (Figures 6 and S6). Additionally, sequencing of rare joints in *Paxx*^{-/-} *Xlf*^{-/-} pro-B cells revealed increased end resection and micro-homology usage reminiscent of joints found in the absence of core NHEJ factors (Figure S4) (Deriano and Roth, 2013). Therefore, PAXX promotes the joining of coding and signal ends during V(D)J recombination (Figure 7).

The observation that *Xlf*^{-/-} cells are more radiosensitive than *Paxx*^{-/-} cells (Figure 1D) is consistent with our findings that PAXX and XLF have redundant (i.e., end-joining) and non-redundant (i.e., end-stabilization) functions in the context of the repair of RAG-generated DNA breaks. Thus, upon irradiation-induced DSBs, XLF-deficient cells might suffer from defects in both end-stabilization and end-joining whereas PAXX-deficient cells only display defects in end-joining. The more severe radiosensitivity observed in PAXX/XLF-deficient cells is congruent with a complete lack of DNA end joining in these cells. More surprising is our finding that PAXX/XLF-deficient pro-B cells have increased sensitivity to radiation-induced DNA damage than XRCC4-deficient pro-B cells. This result is reminiscent of the observation that XRCC4/XLF-deficient cells are more sensitive to hydroxyurea and zeocin than XRCC4-deficient cells (Roy et al., 2015). Considering that XLF function in stabilizing and joining DNA ends depends on XRCC4, these data indicate that XLF also plays XRCC4-independent function(s) during DSB repair.

The question remains of how PAXX rejoins RAG-cleaved DNA ends and whether this function is regulated. In response to genotoxic stress, ATM phosphorylates hundreds of proteins active in different aspects of the DNA damage response (Matsuoka et al., 2007). It will be interesting to test whether ATM regulates, possibly through phosphorylation, PAXX in response to RAG cleavage. This would potentially explain the severe end-joining defect observed in ATM/XLF cells (Kumar et al., 2014; Zha

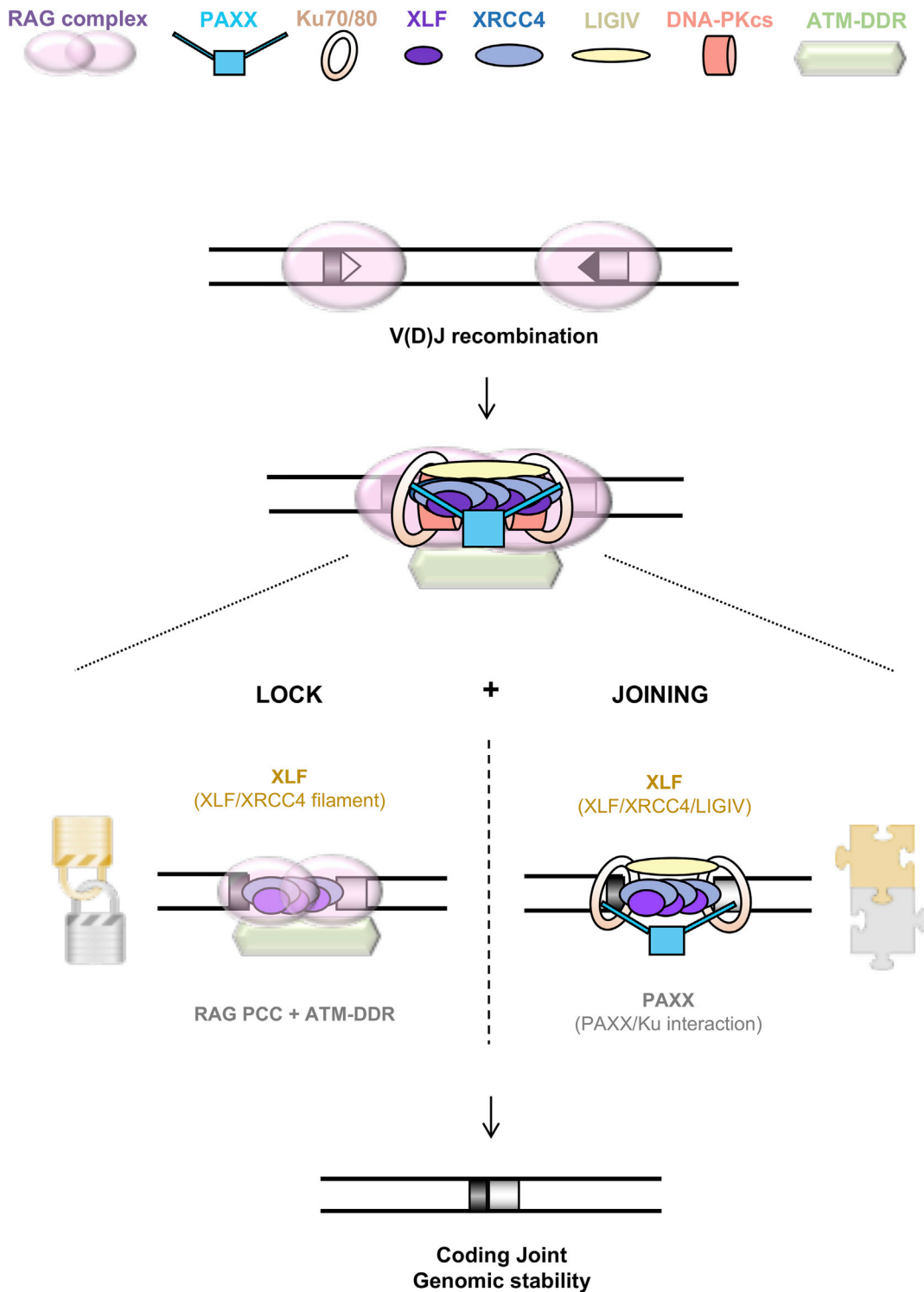


Figure 7. A Lock-and-Join Model for Repair of DNA Ends During V(D)J Recombination

During V(D)J recombination, coding ends stay associated with the RAG proteins in a post-cleavage complex (RAG-PCC). Together with the ATM-dependent DNA damage response (ATM-DDR), the RAG-PCC contributes to stabilization (locking) of broken DNA ends. In the absence of RAG or ATM-DDR, XLF, most likely through the formation of XLF-XRCC4 hetero-filaments ensure tethering of DNA ends and the formation of CJs. Unlike its paralog XLF, PAXX does not seem to play major roles in locking broken coding ends. Instead, PAXX contributes to their joining, possibly by promoting the stimulation of the XRCC4/Ligase 4 enzymatic complex. This end-joining function is redundant with XLF and requires interaction with Ku.

et al., 2011). XLF has been proposed to stimulate DSB ligation by promoting the adenylation of XRCC4/Ligase 4 (Riballo et al., 2009), and, in the absence of XLF, PAXX could potentially act as substitute for XLF in stimulating Ligase 4. Indeed, in vitro, both PAXX and XLF have been reported to stimulate XRCC4/Ligase 4-mediated end joining at certain types of DNA ends (Ochi et al., 2015; Xing et al., 2015). More work is needed to parse whether PAXX participates in joining DNA ends by directly stimulating Ligase 4 catalysis, promoting the assembly of core NHEJ factors to chromatin (Ochi et al., 2015), and/or promoting a yet undescribed mechanism.

Genetic mouse models and human patients with hereditary defects in NHEJ factors suffer from a large variety of defects, including radiation sensitivity, immunodeficiency, developmental defects, and predisposition to cancer (Revy et al., 2005; Rooney et al., 2004). It will be interesting to see whether *Paxx* knockout and *Paxx/Xlf* double knockout animals harbor such developmental and immunological defects and to what extent.

EXPERIMENTAL PROCEDURES

CRISPR/Cas9 Gene Knockout in pro-B Cells

Please refer to Table S1 for a complete list of *v-abl* pro-B cell lines used in this study. All animal experiments were performed in accordance with the guidelines of the institutional animal care committee of Institut Pasteur/CEEA Ile-de-France-Paris1 under the protocol no. 2012-0036.

Generation of *Paxx*^{-/-} pro-B Cell Lines

v-abl pro-B cell lines were cultured in RPMI/15%FBS/Pen-Strep as previously reported (Lescale et al., 2016). Small-guide RNAs (sgRNAs) were designed with CRISPR DESIGN online tool (Zhang lab) and cloned into a MLM3636 vector. sgRNA-P1: 5'-CAGCAGGGCGGTCTCGCCG-3', sgRNA-P2: 5'-ATGCAACCTAGAGAGCGGC-3', and sgRNA-P3: 5'-ACTAGAGTTGAAGTCGTG-3'. Two strategies were set up to inactivate *Paxx* gene. The first one deleted all of exons 1–4 (sgRNA-P1 + sgRNA-P2), removing the ATG start codon. The second strategy (sgRNA-P2 + sgRNA-P3) deleted part of exons 1–4, contributing to β sheets 3–7 and α helices 1–3 (Xing et al., 2015) and led to frameshift and/or stop mutations 3' of sgRNA-P2 in all clones used in this study (Figure 1 and Table S1). 15 million pro-B cells were transfected using the Cell Line Nucleofector Kit V from Lonza (program X-001, Amaxa Nucleofector Technology) and 10 μg of plasmid. Electroporated cells were resuspended in regular RPMI/FBS/Pen-Strep medium at a density of 1 × 10⁶ cells/ml. After 24–48 hr recovery, cells were isolated in 96-well plates by single-cell sorting with an ARIA II (BD Biosciences). After 1 week, clones were screened by PCR using primers 5'-ATGAGAGACTCCCTGGACA 3' and 5'-ACCCGGAACAATGTCAACC-3' amplifying around the expected deletion site. The absence of the protein was confirmed by western blot (see Figure 1).

Generation of *Paxx*^{-/-} *Atm*^{-/-} pro-B cell Lines

Paxx^{-/-} *Atm*^{-/-} pro-B cell clones were generated by deleting *Paxx* from established *Atm*^{-/-} pro-B cell lines as described previously.

Generation of *Paxx*^{-/-} *Rag2*^{cl/c} pro-B Cell Lines

Paxx^{-/-} *Rag2*^{cl/c} pro-B cell clones were generated by deleting *Paxx* from established *Rag2*^{cl/c} pro-B cell lines as described previously.

Generation of *Xlf*^{-/-} and *Paxx*^{-/-} *Xlf*^{-/-} pro-B Cell Lines

Xlf^{-/-} and *Paxx*^{-/-} *Xlf*^{-/-} pro-B cell clones were generated by deleting *Xlf* exon 1 from WT and *Paxx*^{-/-} pro-B cells, respectively, using sgRNA-X1: 5'-TTAGCATAACCAACTTC-3' and sgRNA-X2: 5'-CACCAACAGGTACTCATA-3'. Clones were screened by PCR using primers 5'-ACAAGTCTAATGCACCCA-3' and 5'-GGGTTGCAGCCTTAGAAAAGT-3'.

Generation of *Xrcc4*^{-/-} pro-B Cell Lines

Xrcc4^{-/-} pro-B cell clones were generated by deleting part of *Xrcc4* exon 3 from WT pro-B cells using sgRNA-Xr1: 5'-GAATGTATAACAGGAGACGG-3'

and sgRNA-Xr2: 5'-GCCGAGACTCCTTAGAAAAG-3'. Clones were screened by PCR using primers 5'-CCCTCACAGAAACACAACCTCA-3' and 5'-CAAGGAGGTGGCCACTAGTT-3'.

Irradiation Sensitivity Assay

Pro-B cells were plated in 12-well plates at 0.5 × 10⁶ cells/ml. Cells were irradiated at 0, 1, 2.5, or 5 Gy (Faxitron X-ray). 3 days after irradiation, viable cells were counted with a Casy cell counter (Roche). The percentages of viable cells compared to non-irradiated control cells were determined. Experiments were performed using two independent cell lines of each genotype and were repeated three times (see Table S2).

Western Blotting

Cells were lysed using RIPA cell lysis reagent (Thermo Fisher Scientific) and protease inhibitors cocktail (Sigma-Aldrich). Equal amounts of proteins were subjected to SDS-PAGE on 4%–12% Bis-Tris gel. Proteins were transferred onto a nitrocellulose membrane (Life Technologies) using the iBlot apparatus (P3 program, 7 min transfer, Invitrogen). The membrane was exposed to Ponceau red staining (Sigma-Aldrich), washed, incubated in 5% non-fat dried milk in TBS containing 0.05% Tween-20 buffer for 1 hr at room temperature (RT), and subsequently incubated overnight at 4°C with primary antibody against PAXX protein (ab126353, 1:1000 dilution, Abcam) and γ-Tubulin protein (T6557, 1:20,000 dilution, Sigma-Aldrich). The membrane was then washed three times with TBS-Tween before incubation for 1 hr at RT with HRP-conjugated antibodies (7,074 or 7,076, 1:20,000 dilution, Cell Signaling Technology). Immune complexes were detected with WesternBright Sirius substrate (Advanta).

V(D)J Recombination Assays

The pMX-INV, pMX-DEL^{CJ}, or pMX-DEL^{SJ} substrates were introduced in pro-B cell lines through retroviral infection, and cells that had integrated the recombination substrate were enriched based on hCD4 expression (Bredemeyer et al., 2006; Liang et al., 2002). For V(D)J recombination assay, *v-abl*-transformed, *Bcl2*/pMX-INV-infected pro-B cells (10⁶/ml) were treated with 3 μM of the *v-abl* kinase inhibitor STI571 (referred to as ABLki in this study, Novartis) and assayed for rearrangement by FACS analysis of GFP expression or Southern blotting at 0, 72, and/or 96 hr. In some experiments, the ATM kinase inhibitor KU55933 was added at 15 μM together with STI571. For FACS analysis, V(D)J recombination efficiency was scored as the percentage of GFP-positive cells among hCD4-positive cells (human CD4-PE, Miltenyi Biotec, 1:20 dilution). The pMX-INV-mCherry substrate was built by replacing the inverted GFP cDNA from pMX-RSS-GFP/IRE5-hCD4 (pMX-INV) by an inverted mCherry cDNA.

Southern Blot

Southern blots were performed as previously described (Lescale et al., 2016). 50 μg of gDNA from untreated, ABLki-treated and ABLki/ATMki-treated pro-B cell lines were digested overnight with EcoRV for both pMX-DEL^{CJ} and pMX-DEL^{SJ} and with EcoRV or EcoRV/NcoI for pMX-INV. Digested gDNA samples were run overnight on an agarose gel, denatured by incubating the gel with 0.5 M NaOH/0.6M NaCl for 1 hr, and then transferred overnight on a Zeta-Probe GT nylon membrane (BioRad). DNA was cross-linked on the membrane using a UV Cross-linker CL-508 (Uvitec Cambridge). Blots were incubated at 42°C in pre-hybridization buffer for at least 1 hr and then overnight in hybridization buffer containing 32^P-CTP-labeled C4 probe (Bredemeyer et al., 2006). Blots were washed in 2XSSC/0.1% SDS at 65°C and exposed to a Storage Phosphor Screen (GE Healthcare) for 2 to 5 days. The screen was then scanned using a Storm 860 PhosphorImager (Molecular Dynamics).

PCR Analysis of V(D)J Recombination Products

pMX-DEL^{CJ} CJs, pMX-DEL^{SJ} SJs, and pMX-INV HJs were amplified using pC (GCACGAAGTCTTGAGACCT) and IRES-REV5 (CTCGACTAAACACATG TAAAGC) oligonucleotides. pMX-INV CJs were amplified using pA (CACAA CATCGAGGACGG) and IRES-REV5 primers as previously described (Bredemeyer et al., 2006; Helmink et al., 2011). *Ii-2* gene was amplified using IMR42 (CTAGGCCACAGAATTGAAAGATCT) and IMR43 (GTAGGTG GAAATTCTAGCATGATGC) primers and was used as loading control. pMX-DEL^{SJ} SJ PCR products were incubated with the restriction enzyme ApaLI

(New England Biolabs) for 2 hr at 37°C. pMX-DEL^{SJ} SJs were cloned using TOPO TA Cloning kit (Life Technologies) following the manufacturer's instructions and analyzed with Sanger Sequencing using T3 (AATTAACCCCTCAC TAAAGGGA) and T7 (TAATACGACTCACTATAGG) primers.

Endogenous *V_{K6-29}/J_{K1}* coding and HJs were amplified as previously described (Bredemeyer et al., 2006). 500 ng of genomic DNA was amplified using ρ KJa (GGAGAGTGCCAGAATCTGGTTTCAG) and ρ K6a (TGCATGTCA GAGGCACAACACTG) primers for HJ and ρ KJa2 (GCCACAGACATAGA CAACGGAA) and ρ K6d (GAAATACATCAGACCAGCATGG) primers for C.J. Serial 4-fold dilutions of this reaction were amplified using ρ KJa and ρ K6b (CTACCAAACCTTTGCAACACACAGGC) primers for HJ and ρ KJa2 and ρ K6c (GTTGCTGTGGTTGTCTGGTG) primers for C.J.

Immunofluorescence on Interphase Nuclei

After 3 days of treatment with ABLki, pro-B cell lines were adhered to poly-L lysine-coated coverslips and stained as previously described (Chaumeil et al., 2013; Lescalet et al., 2016). Cells were fixed with 4% paraformaldehyde/PBS for 10 min at RT and permeabilized for 5 min with 0.4% Triton/PBS on ice. Immunofluorescence was performed after 30 min blocking in 2.5% BSA/10% goat serum/0.1% Tween-20/PBS, with a primary antibody against 53BP1 (NB100-304SS, 1:600 dilution, Novus Biologicals) and a secondary goat-anti-rabbit antibody (Alexa Fluor 594, 1:900 dilution; Life Technologies) in blocking solution for 1 hr each at RT. Cells were washed three times with 0.5% BSA/0.1% Tween-20/PBS after both primary and secondary antibody incubations. Finally, slides were mounted in ProLong Gold (Life Technologies) containing DAPI to counterstain total DNA. Cells were imaged in 3D (nine z stacks of 0.5 μ m) using a Zeiss AxioImager Z2 microscope and the Metacyte automated capture system (Metasystems). 53BP1 foci were counted using a custom Metacyte classifier. >10,000 nuclei were counted for each genotype (see Table S3).

PAXX Expression Vectors

Plasmids encoding for GFP-tagged PAXX have been described previously (Ochi et al., 2015). DNA encoding mRuby2-tagged PAXX was synthesized and cloned into pcDNA3.1/Zeo(+) vector (Life Technologies). S184E mutation was introduced by site-directed mutagenesis (Agilent Technologies). Plasmids were transfected into 293FT cells using Lipofectamine 2000 (Life Technologies) for subsequent immunoprecipitation experiments.

Immunoprecipitation

GFP pull-downs were carried out in 293FT cells exactly as previously described (Blackford et al., 2015). Antibody recognizing Ku80 (MS-285-P1, Thermo Scientific) was diluted 1:2,000 for western blotting experiments.

PAXX Complementation of *v-abl* pro-B Cells

pMX-INV-GFP/mCherry pro-B cells were transfected with plasmids encoding for PAXX and mutated PAXX using the Cell Line Nucleofector Kit V from Lonza using the same conditions as for the previously described CRISPR/Cas9 gene knockout strategy. Cells were left to recover in fresh media for 6 hr and subsequently treated with ABLki and assayed for V(D)J recombination by FACS analysis as previously described.

Statistics

All statistical analyses were performed using a non-parametric Mann-Whitney test. In all statistical tests, $p < 0.05$ were taken to be significant (*, $0.01 \leq p < 0.05$; **, $0.001 \leq p < 0.01$; ***, $p < 0.001$).

SUPPLEMENTAL INFORMATION

Supplemental Information contains six figures and four tables and can be found with this article online at <http://dx.doi.org/10.1016/j.celrep.2016.08.069>.

AUTHOR CONTRIBUTIONS

C.L. and H.L.H. performed the experiments. J.J.B. designed and generated sgRNA-expressing vectors. W.Y. generated *Xrcc4*^{-/-} pro-B cell clones. L.B.

and A.J. contributed to experiments. C.C. generated the mCherry-pMX-INV substrate. R.S. generated the mRuby2-PAXX-S184E construct. B.R.-S.-M. provided the sgRNA-CRISPR/Cas9 vector targeting *Xlf*. A.N.B., G.B., and S.P.J. provided the PAXX-expressing vectors, performed PAXX/Ku immunoprecipitations, and commented on the manuscript. C.L., H.L.H., and L.D. designed the study, analyzed the data, and wrote the manuscript.

ACKNOWLEDGMENTS

We thank the Pasteur Cytometry Platform and the Pasteur Center for Human Immunology for their help. We thank Shauna Katz for editing the manuscript. The Jackson Laboratory is funded by Cancer Research UK program grant C6/A18796 and the European Research Council. Core infrastructure funding is provided by CRUK (C6946/A14492) and the Wellcome Trust (WT092096). S.P.J. receives his salary from the University of Cambridge, which is supplemented by CRUK. G.B. and A.N.B. are supported by CRUK (C6/A18796). The L.D. laboratory is funded by the Institut Pasteur as well as the European Research Council under the ERC starting grant agreement no. 310917.

Received: June 22, 2016

Revised: August 2, 2016

Accepted: August 23, 2016

Published: September 2, 2016

REFERENCES

- Agrawal, A., and Schatz, D.G. (1997). RAG1 and RAG2 form a stable post-cleavage synaptic complex with DNA containing signal ends in V(D)J recombination. *Cell* 89, 43–53.
- Andres, S.N., Modesti, M., Tsai, C.J., Chu, G., and Junop, M.S. (2007). Crystal structure of human XLF: a twist in nonhomologous DNA end-joining. *Mol. Cell* 28, 1093–1101.
- Bassing, C.H., Swat, W., and Alt, F.W. (2002). The mechanism and regulation of chromosomal V(D)J recombination. *Cell* 109 (Suppl), S45–S55.
- Blackford, A.N., Nieminuszczy, J., Schwab, R.A., Galanty, Y., Jackson, S.P., and Niedzwiedz, W. (2015). TopBP1 interacts with BLM to maintain genome stability but is dispensable for preventing BLM degradation. *Mol. Cell* 57, 1133–1141.
- Blunt, T., Finnie, N.J., Taccioli, G.E., Smith, G.C.M., Demengeot, J., Gottlieb, T.M., Mizuta, R., Varghese, A.J., Alt, F.W., Jeggo, P.A., and Jackson, S.P. (1995). Defective DNA-dependent protein kinase activity is linked to V(D)J recombination and DNA repair defects associated with the murine scid mutation. *Cell* 80, 813–823.
- Bogue, M.A., Jhappan, C., and Roth, D.B. (1998). Analysis of variable (diversity) joining recombination in DNA-dependent protein kinase (DNA-PK)-deficient mice reveals DNA-PK-independent pathways for both signal and coding joint formation. *Proc. Natl. Acad. Sci. USA* 95, 15559–15564.
- Bredemeyer, A.L., Sharma, G.G., Huang, C.-Y., Helmink, B.A., Walker, L.M., Khor, K.C., Nuskey, B., Sullivan, K.E., Pandita, T.K., Bassing, C.H., and Sleckman, B.P. (2006). ATM stabilizes DNA double-strand-break complexes during V(D)J recombination. *Nature* 442, 466–470.
- Callebaut, I., Malivert, L., Fischer, A., Morion, J.P., Revy, P., and de Villartay, J.P. (2006). Cernunnos interacts with the XRCC4 x DNA-ligase IV complex and is homologous to the yeast nonhomologous end-joining factor Nej1. *J. Biol. Chem.* 281, 13857–13860.
- Chaumeil, J., Micsinai, M., and Skok, J.A. (2013). Combined immunofluorescence and DNA FISH on 3D-preserved interphase nuclei to study changes in 3D nuclear organization. *J. Vis. Exp.* 72, e50087.
- Craxton, A., Somers, J., Munnur, D., Jukes-Jones, R., Cain, K., and Malewicz, M. (2015). XLS (c9orf142) is a new component of mammalian DNA double-stranded break repair. *Cell Death Differ.* 22, 890–897.
- Deriano, L., and Roth, D.B. (2013). Modernizing the nonhomologous end-joining repertoire: alternative and classical NHEJ share the stage. *Annu. Rev. Genet.* 47, 433–455.

- Gao, Y., Sun, Y., Frank, K.M., Dikkes, P., Fujiwara, Y., Seidl, K.J., Sekiguchi, J.M., Rathbun, G.A., Swat, W., Wang, J., et al. (1998). A critical role for DNA end-joining proteins in both lymphogenesis and neurogenesis. *Cell* 95, 891–902.
- Gottlieb, T.M., and Jackson, S.P. (1993). The DNA-dependent protein kinase: requirement for DNA ends and association with Ku antigen. *Cell* 72, 131–142.
- Hammel, M., Rey, M., Yu, Y., Mani, R.S., Classen, S., Liu, M., Pique, M.E., Fang, S., Mahaney, B.L., Weinfeld, M., et al. (2011). XRCC4 protein interactions with XRCC4-like factor (XLF) create an extended grooved scaffold for DNA ligation and double strand break repair. *J. Biol. Chem.* 286, 32638–32650.
- Harrigan, J.A., Belotserkovskaya, R., Coates, J., Dimitrova, D.S., Polo, S.E., Bradshaw, C.R., Fraser, P., and Jackson, S.P. (2011). Replication stress induces 53BP1-containing OPT domains in G1 cells. *J. Cell Biol.* 193, 97–108.
- Helmkink, B.A., and Sleckman, B.P. (2012). The response to and repair of RAG-mediated DNA double-strand breaks. *Annu. Rev. Immunol.* 30, 175–202.
- Helmkink, B.A., Tubbs, A.T., Dorsett, Y., Bednarski, J.J., Walker, L.M., Feng, Z., Sharma, G.G., McKinnon, P.J., Zhang, J., Bassing, C.H., and Sleckman, B.P. (2011). H2AX prevents CtIP-mediated DNA end resection and aberrant repair in G1-phase lymphocytes. *Nature* 469, 245–249.
- Hickson, I., Zhao, Y., Richardson, C.J., Green, S.J., Martin, N.M., Orr, A.I., Reaper, P.M., Jackson, S.P., Curtin, N.J., and Smith, G.C. (2004). Identification and characterization of a novel and specific inhibitor of the ataxia-telangiectasia mutated kinase ATM. *Cancer Res.* 64, 9152–9159.
- Hiom, K., and Gellert, M. (1998). Assembly of a 12/23 paired signal complex: a critical control point in V(D)J recombination. *Mol. Cell* 1, 1011–1019.
- Kumar, V., Alt, F.W., and Oksenyk, V. (2014). Functional overlaps between XLF and the ATM-dependent DNA double strand break response. *DNA Repair (Amst.)* 16, 11–22.
- Lescale, C., and Deriano, L. (2016). V(D)J Recombination: Orchestrating Diversity without Damage. *Encyclopedia of Cell Biology* 3, 550–566.
- Lescale, C., Abramowski, V., Bedora-Faure, M., Murigneux, V., Vera, G., Roth, D.B., Revy, P., de Villartay, J.P., and Deriano, L. (2016). RAG2 and XLF/Cernunnos interplay reveals a novel role for the RAG complex in DNA repair. *Nat. Commun.* 7, 10529.
- Li, Z., Otevrel, T., Gao, Y., Cheng, H.-L., Seed, B., Stamato, T.D., Taccioli, G.E., and Alt, F.W. (1995). The XRCC4 gene encodes a novel protein involved in DNA double-strand break repair and V(D)J recombination. *Cell* 83, 1079–1089.
- Li, G., Alt, F.W., Cheng, H.L., Brush, J.W., Goff, P.H., Murphy, M.M., Franco, S., Zhang, Y., and Zha, S. (2008a). Lymphocyte-specific compensation for XLF/cernunnos end-joining functions in V(D)J recombination. *Mol. Cell* 31, 631–640.
- Li, Y., Chirgadze, D.Y., Bolanos-Garcia, V.M., Sibanda, B.L., Davies, O.R., Ahnesorg, P., Jackson, S.P., and Blundell, T.L. (2008b). Crystal structure of human XLF/Cernunnos reveals unexpected differences from XRCC4 with implications for NHEJ. *EMBO J.* 27, 290–300.
- Liang, H.E., Hsu, L.Y., Cado, D., Cowell, L.G., Kelseo, G., and Schlessel, M.S. (2002). The “dispensable” portion of RAG2 is necessary for efficient V-to-DJ rearrangement during B and T cell development. *Immunity* 17, 639–651.
- Lieber, M.R. (2010). The mechanism of double-strand DNA break repair by the nonhomologous DNA end-joining pathway. *Annu. Rev. Biochem.* 79, 181–211.
- Mahaney, B.L., Hammel, M., Meek, K., Tainer, J.A., and Lees-Miller, S.P. (2013). XRCC4 and XLF form long helical protein filaments suitable for DNA end protection and alignment to facilitate DNA double strand break repair. *Biochem. Cell Biol.* 97, 31–41.
- Matsuoka, S., Ballif, B.A., Smogorzewska, A., McDonald, E.R., 3rd, Hurov, K.E., Luo, J., Bakalarski, C.E., Zhao, Z., Solimini, N., Lerenthal, Y., et al. (2007). ATM and ATR substrate analysis reveals extensive protein networks responsive to DNA damage. *Science* 316, 1160–1166.
- Mizuta, R., Cheng, H.L., Gao, Y., and Alt, F.W. (1997). Molecular genetic characterization of XRCC4 function. *Int. Immunol.* 9, 1607–1613.
- Muljo, S.A., and Schlessel, M.S. (2003). A small molecule Abl kinase inhibitor induces differentiation of Abelson virus-transformed pre-B cell lines. *Nat. Immunol.* 4, 31–37.
- Ochi, T., Wu, Q., and Blundell, T.L. (2014). The spatial organization of non-homologous end joining: from bridging to end joining. *DNA Repair (Amst.)* 17, 98–109.
- Ochi, T., Blackford, A.N., Coates, J., Jhujh, S., Mehmood, S., Tamura, N., Travers, J., Wu, Q., Draviam, V.M., Robinson, C.V., et al. (2015). DNA repair. PAXX, a paralog of XRCC4 and XLF, interacts with Ku to promote DNA double-strand break repair. *Science* 347, 185–188.
- Ramsden, D.A., Paull, T.T., and Gellert, M. (1997). Cell-free V(D)J recombination. *Nature* 388, 488–491.
- Reid, D.A., Keegan, S., Leo-Macias, A., Watanabe, G., Strande, N.T., Chang, H.H., Oksuz, B.A., Fenyo, D., Lieber, M.R., Ramsden, D.A., and Rothenberg, E. (2015). Organization and dynamics of the nonhomologous end-joining machinery during DNA double-strand break repair. *Proc. Natl. Acad. Sci. USA* 112, E2575–E2584.
- Revy, P., Buck, D., le Deist, F., and de Villartay, J.P. (2005). The repair of DNA damages/modifications during the maturation of the immune system: lessons from human primary immunodeficiency disorders and animal models. *Adv. Immunol.* 87, 237–295.
- Riballo, E., Woodbine, L., Stiff, T., Walker, S.A., Goodarzi, A.A., and Jeggo, P.A. (2009). XLF-Cernunnos promotes DNA ligase IV-XRCC4 re-adenylation following ligation. *Nucleic Acids Res.* 37, 482–492.
- Rooney, S., Chaudhuri, J., and Alt, F.W. (2004). The role of the non-homologous end-joining pathway in lymphocyte development. *Immunol. Rev.* 200, 115–131.
- Ropars, V., Drevet, P., Legrand, P., Baconnais, S., Amram, J., Faure, G., Márquez, J.A., Piétrement, O., Guerois, R., Callebaut, I., et al. (2011). Structural characterization of filaments formed by human Xrcc4-Cernunnos/XLF complex involved in nonhomologous DNA end-joining. *Proc. Natl. Acad. Sci. USA* 108, 12663–12668.
- Roy, S., de Melo, A.J., Xu, Y., Tadi, S.K., Negrel, A., Hendrickson, E., Modesti, M., and Meek, K. (2015). XRCC4/XLF interaction is variably required for DNA repair, and is not required for Ligase IV stimulation. *Mol. Cell Biol.*
- Schatz, D.G., and Swanson, P.C. (2011). V(D)J recombination: mechanisms of initiation. *Annu. Rev. Genet.* 45, 167–202.
- Schwartz, M., Oren, Y.S., Bester, A.C., Rahat, A., Sfez, R., Yitzchaik, S., de Villartay, J.P., and Kerem, B. (2009). Impaired replication stress response in cells from immunodeficiency patients carrying Cernunnos/XLF mutations. *PLoS ONE* 4, e4516.
- Shinkai, Y., Rathbun, G., Lam, K.-P., Oltz, E.M., Stewart, V., Mendelsohn, M., Charron, J., Datta, M., Young, F., Stall, A.M., et al. (1992). RAG-2-deficient mice lack mature lymphocytes owing to inability to initiate V(D)J rearrangement. *Cell* 68, 855–867.
- Tsai, C.J., Kim, S.A., and Chu, G. (2007). Cernunnos/XLF promotes the ligation of mismatched and noncohesive DNA ends. *Proc. Natl. Acad. Sci. USA* 104, 7851–7856.
- Vera, G., Rivera-Munoz, P., Abramowski, V., Malivert, L., Lim, A., Bole-Feysot, C., Martin, C., Florin, B., Latour, S., Revy, P., and de Villartay, J.P. (2013). Cernunnos deficiency reduces thymocyte life span and alters the T cell repertoire in mice and humans. *Mol. Cell Biol.* 33, 701–711.
- Xing, M., Yang, M., Huo, W., Feng, F., Wei, L., Jiang, W., Ning, S., Yan, Z., Li, W., Wang, Q., et al. (2015). Interactome analysis identifies a new paralogue of XRCC4 in non-homologous end joining DNA repair pathway. *Nat. Commun.* 6, 6233.
- Zha, S., Guo, C., Boboila, C., Oksenyk, V., Cheng, H.L., Zhang, Y., Wesemann, D.R., Yuen, G., Patel, H., Goff, P.H., et al. (2011). ATM damage response and XLF repair factor are functionally redundant in joining DNA breaks. *Nature* 469, 250–254.

Cell Reports, Volume 16

Supplemental Information

Specific Roles of XRCC4 Paralogs PAXX and XLF during V(D)J Recombination

Chloé Lescale, Hélène Lenden Hasse, Andrew N. Blackford, Gabriel Balmus, Joy J. Bianchi, Wei Yu, Léa Bacoccina, Angélique Jarade, Christophe Clouin, Rohan Sivapalan, Bernardo Reina-San-Martin, Stephen P. Jackson, and Ludovic Deriano

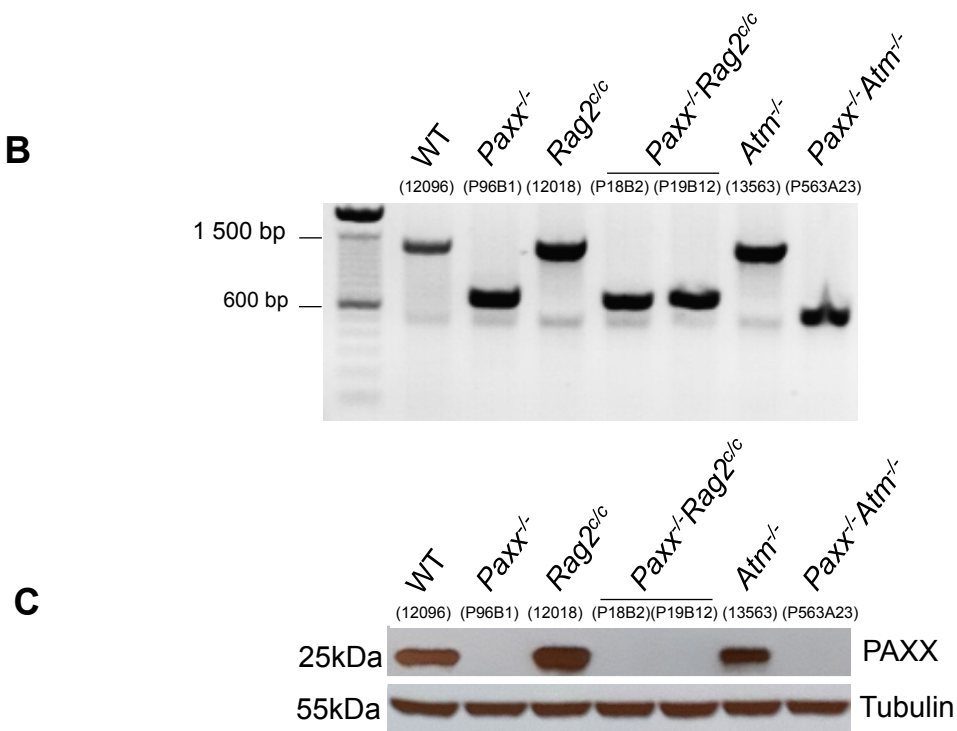
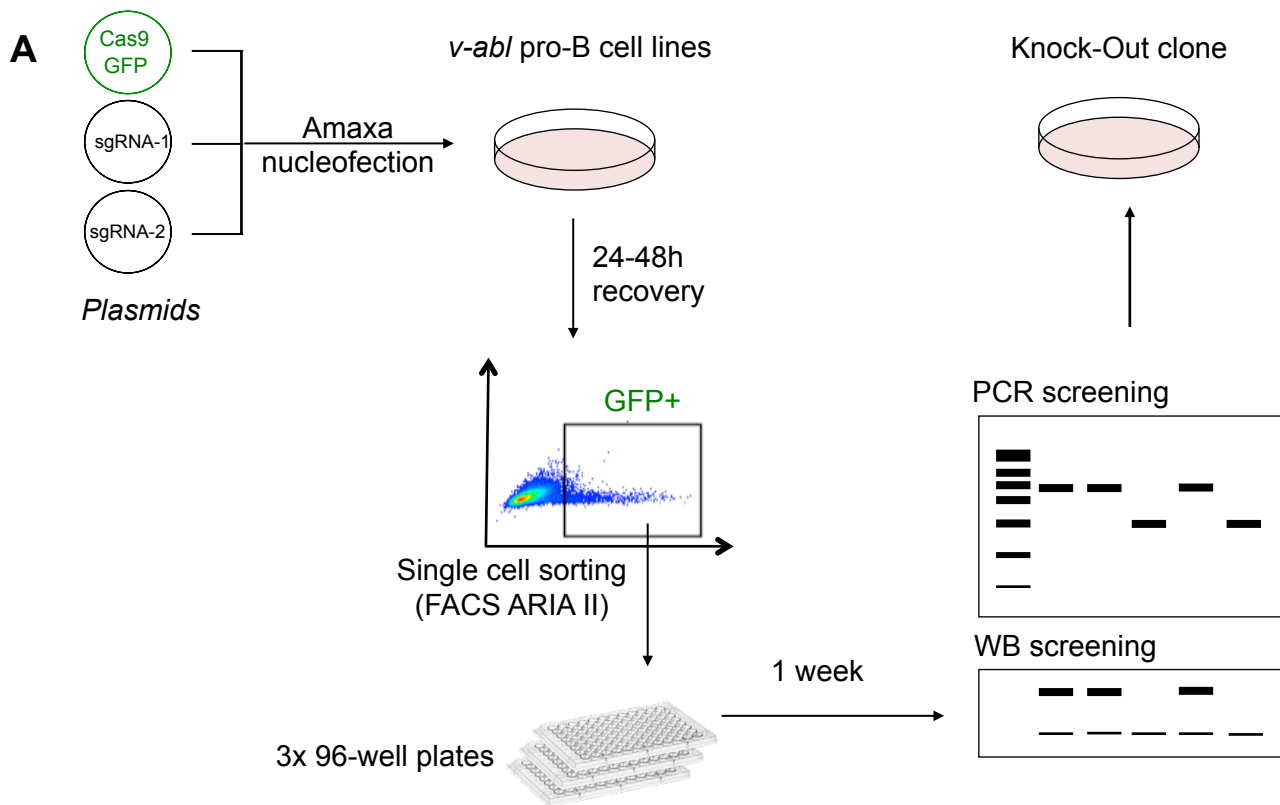


Figure S1. Experimental strategy, Related to Figure 1

- (A) Scheme depicting the experimental strategy for CRISPR/Cas9 genome editing of pro-B cell lines.
 (B) PCR analysis showing the deletion of approximately 626bp in the *Paxx* gene (WT = 1299bp band; *Paxx* KO ≈ 673bp band).
 (C) Western blot showing the absence of the PAXX protein in *Paxx*^{-/-} *Rag2*^{c/c} and *Paxx*^{-/-} *Atm*^{-/-} pro-B cell clones.

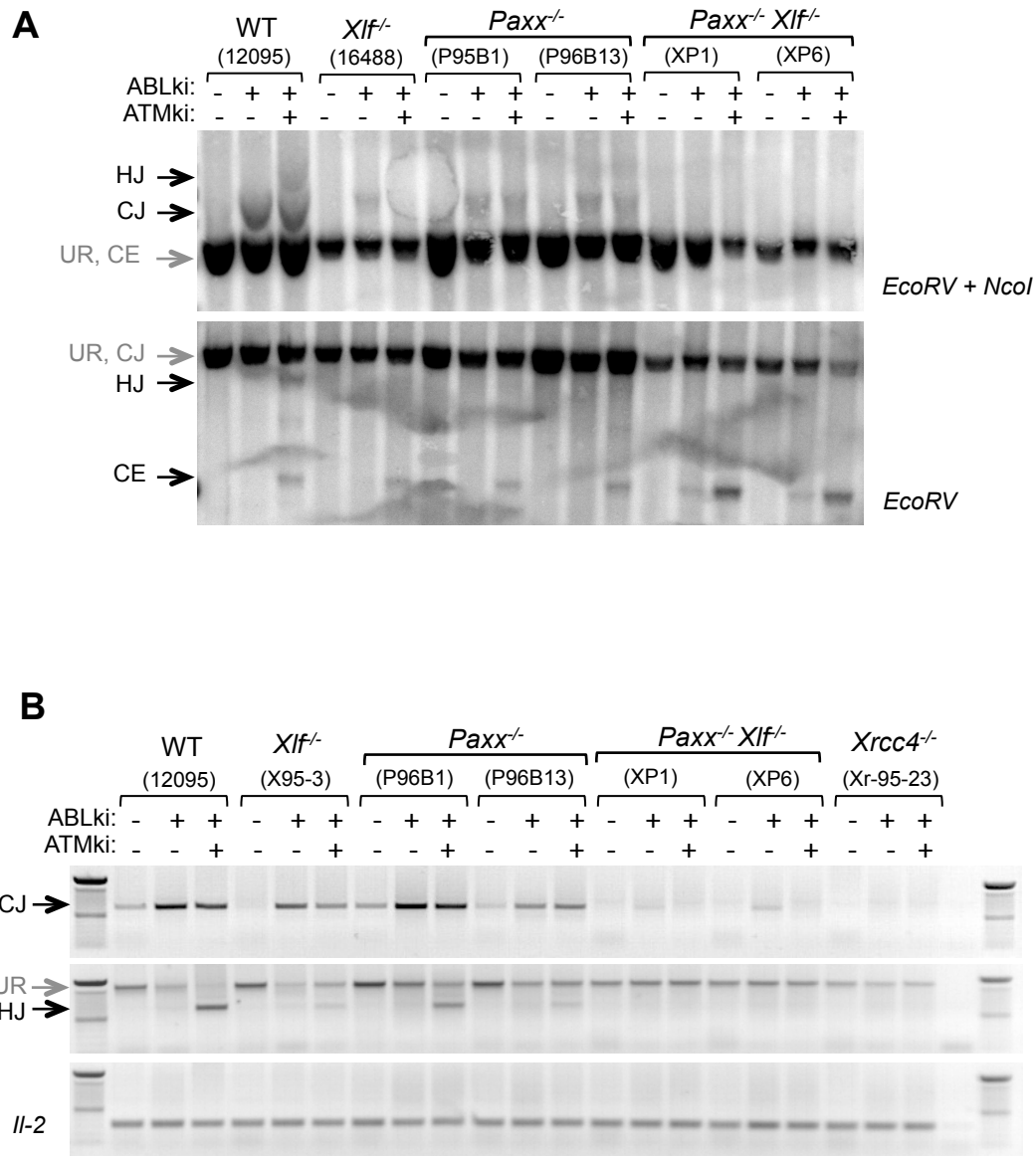


Figure S2. Defective inversional V(D)J recombination in *Paxx*^{-/-} *Xif*^{-/-} B cells, Related to Figure 3

(A) The indicated *v-abl* pro-B cell lines containing the pMX-INV substrate were treated for 72h with ABLki with or without ATMki and assayed by Southern blotting; EcoRV/NcoI digest – C4 probe (top panel) and EcoRV digest – C4 probe (bottom panel).

(B) PCR analysis of pMX-INV coding and hybrid joints from indicated *v-abl* *abl* pro-B cell lines treated for 72h with ABLki with or without ATMki. *Il-2* gene PCR was used as a loading control.

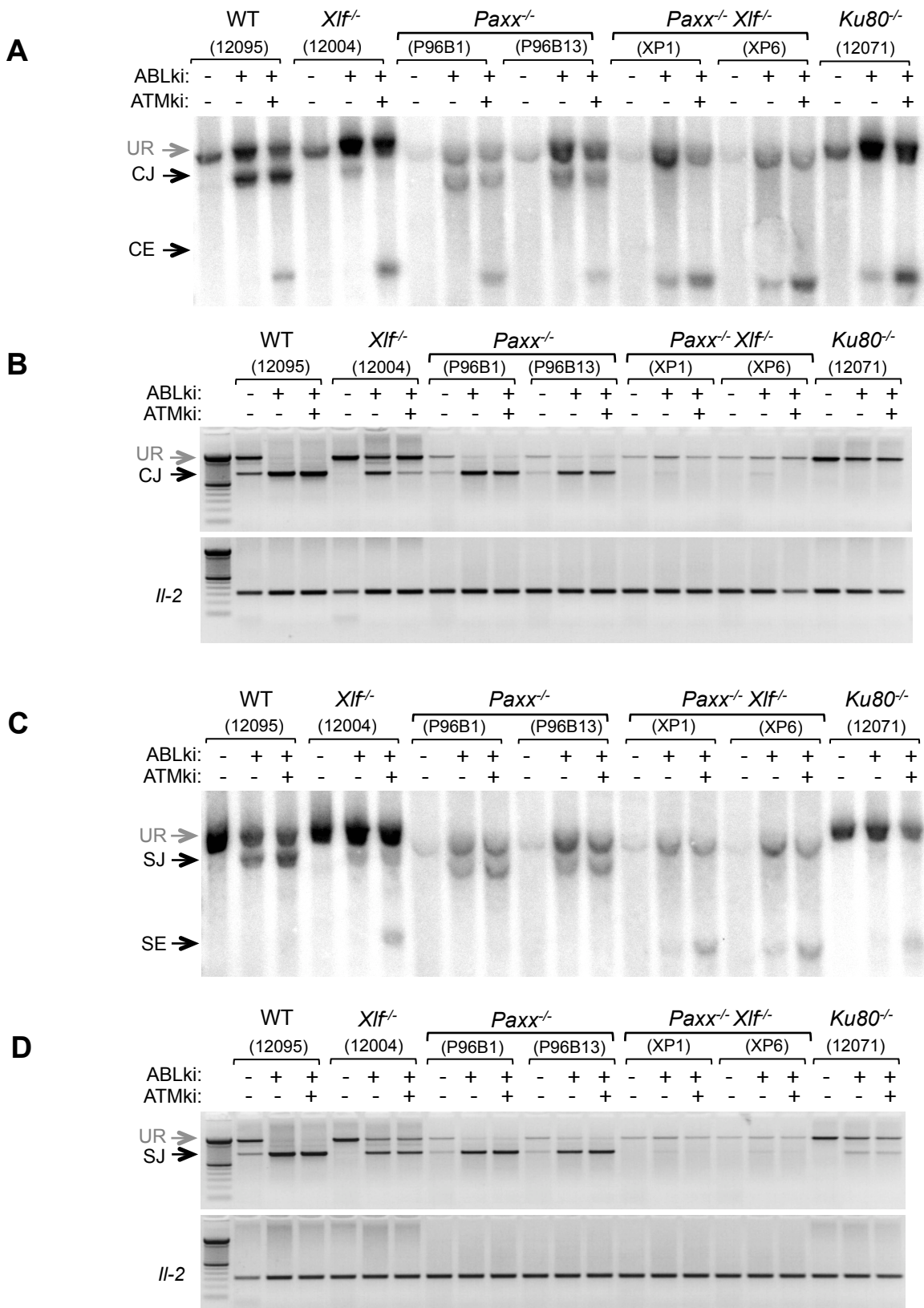


Figure S3. Defective deletional coding and signal joint formation in *Paxx*^{-/-} *Xif*^{-/-} B cells, Related to Figure 4

pMX-DEL^{CJ} (A, B) and pMX-DEL^{SJ} (C, D) *v-abl* pro-B cell lines were treated for 72h with ABLki with or without ATMki. Coding and signal joint formation were assessed by Southern blotting; EcoRV digest – C4 probe (A, C) and by PCR (B, D). *Il-2* gene PCR was used as a loading control (B, D).

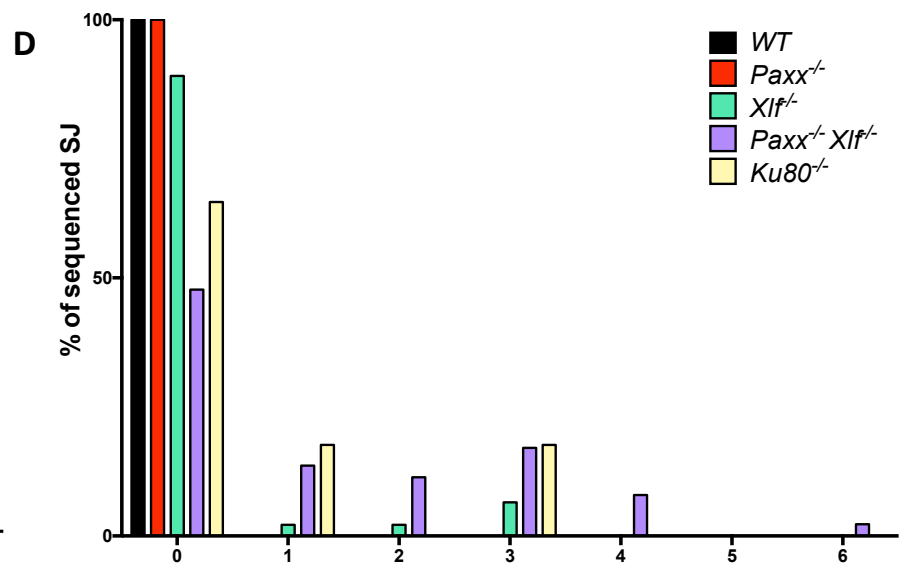
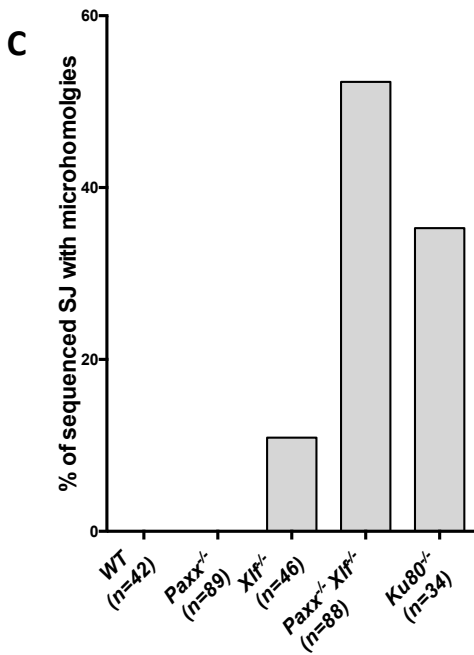
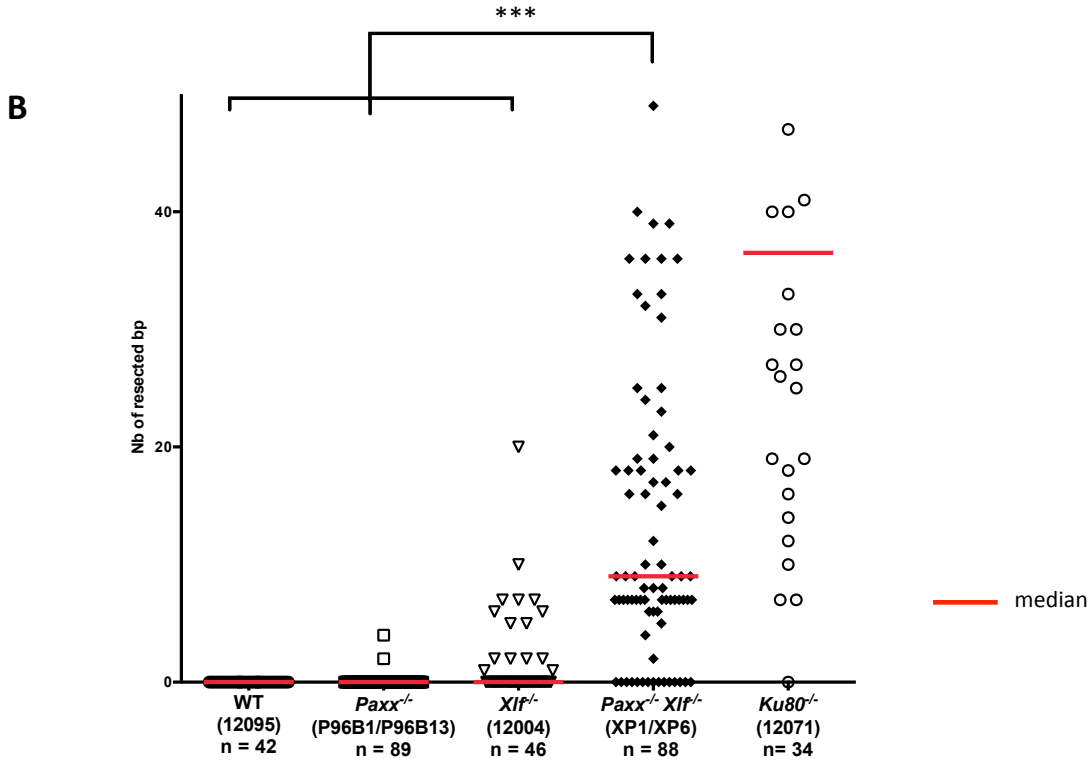
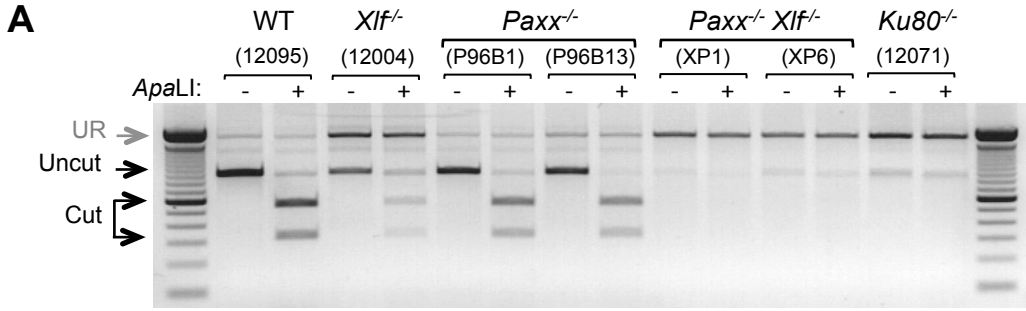


Figure S4. Analysis of signal joints sequences in *v-abl* pMX-DEL^{SJ} pro-B cell lines, Related to Figure 4

(A) PCR products of pMX-DEL^{SJ} signal junctions were digested by *Apa*LI.

(B) Sanger sequencing of PCR amplified signal joints from *v-abl* pro-B cells (See also Table S4).

Number of base-pair deletions is indicated on the y-axis. The horizontal bar represents the median.

The total number of sequenced signal joints (n) is indicated. Outliers (> 49 bp deletion) are not shown but are included in calculation of the median. ***p<0.001.

(C and D) Microhomology utilization in pMX-DEL^{SJ} SJs sequenced from indicated *v-abl* pro-B cell lines. (C) Percentage of sequences with microhomologies \geq 1bp. (D) Microhomology length

distribution among the same sequences.

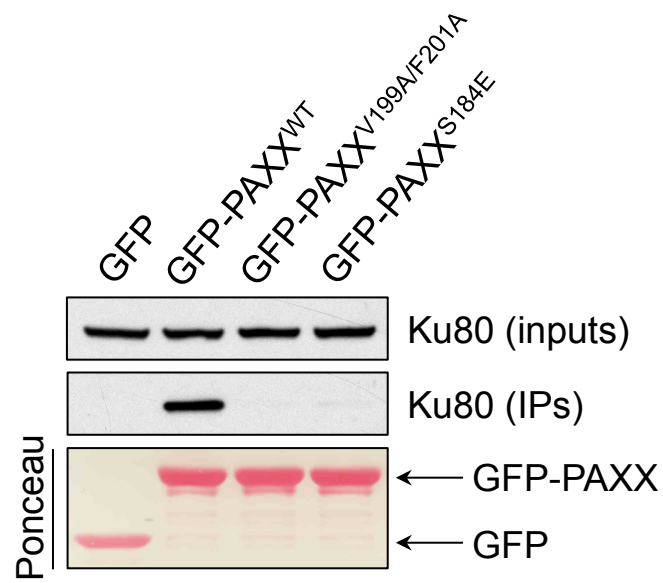


Figure S5. C-terminal PAXX mutations S184E or V199A/F201A similarly abolish the PAXX-Ku interaction, Related to Figure 6

Pulldowns assays from 293FT cells transiently transfected with the indicated plasmids.

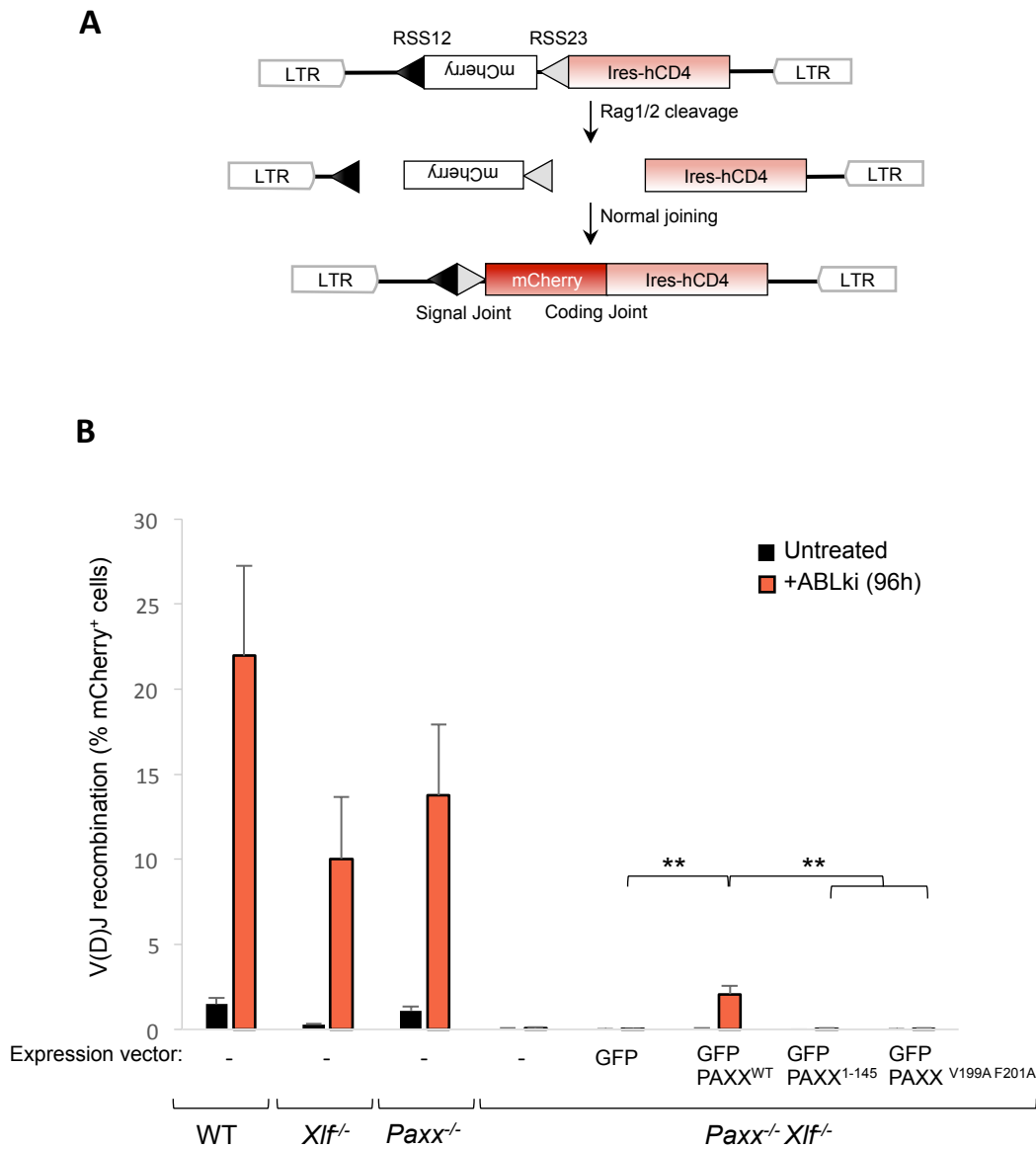


Figure S6. PAXX function in the absence of XLF depends on its interaction with Ku, Related to Figure 6

(A) Schematic representation of pMX-INV-Cherry recombination substrate.

(B) *Paxx*^{-/-} *Xlf*^{-/-} pro-B cell lines (XP1, XP6) were transfected with expression vectors encoding for GFP, GFP-PAXX^{WT}, GFP-PAXX¹⁻¹⁴⁵ or GFP-PAXX^{V199A/F201A}. After 6h recovery, *Paxx*^{-/-} *Xlf*^{-/-} transfected cells, along with control untransfected cells, were treated for 96 hours with ABLki and assayed for pMX-INV-Cherry rearrangement by flow cytometry, with the percentage of mCherry expressing cells indicated. Data represent the means ± SEMs of three experiments with two independent cell lines for *Paxx*^{-/-} *Xlf*^{-/-} cell lines and one for the other cell lines.

Genotype	Cell line #	Generation method	Reference
WT	12096	<i>v-Abl/Bcl2</i> immortalization of bone marrow pro-B cells	Lescale et al., 2016
	12095	<i>v-Abl/Bcl2</i> immortalization of bone marrow pro-B cells	Lescale et al., 2016
<i>Paxx</i>^{-/-}	P96B1	CRISPR-Cas9 genome editing of 12096 cell line	This study
	P96B13	CRISPR-Cas9 genome editing of 12096 cell line	This study
	P95B1	CRISPR-Cas9 genome editing of 12095 cell line	This study
<i>Paxx</i>^{-/-} <i>Xlf</i>^{-/-}	XP1	CRISPR-Cas9 genome editing of P96B1 cell line	This study
	XP6	CRISPR-Cas9 genome editing of P96B1 cell line	This study
<i>Xlf</i>^{-/-}	X95-3	CRISPR-Cas9 genome editing of 12095 cell line	This study
	X95-4	CRISPR-Cas9 genome editing of 12095 cell line	This study
	16488	<i>v-Abl/Bcl2</i> immortalization of bone marrow pro-B cells	This study
	12004	<i>v-Abl/Bcl2</i> immortalization of bone marrow pro-B cells	Lescale et al., 2016
<i>Ku80</i>^{-/-}	12071	<i>v-Abl/Bcl2</i> immortalization of bone marrow pro-B cells	Lescale et al., 2016
<i>Xrcc4</i>^{-/-}	Xr-95-21	CRISPR-Cas9 genome editing of 12095 cell line	This study
	Xr-95-23	CRISPR-Cas9 genome editing of 12095 cell line	This study
<i>Rag2</i>^{c/c}	12018	<i>v-Abl/Bcl2</i> immortalization of bone marrow pro-B cells	Lescale et al., 2016
	12019	<i>v-Abl/Bcl2</i> immortalization of bone marrow pro-B cells	Lescale et al., 2016
<i>Paxx</i>^{-/-} <i>Rag2</i>^{c/c}	P18B2	CRISPR-Cas9 genome editing of 12018 cell line	This study
	P19B12	CRISPR-Cas9 genome editing of 12019 cell line	This study
<i>Atm</i>^{-/-}	13563	<i>v-Abl/Bcl2</i> immortalization of bone marrow pro-B cells	This study
	160	<i>v-Abl/Bcl2</i> immortalization of bone marrow pro-B cells	This study
<i>Paxx</i>^{-/-} <i>Atm</i>^{-/-}	P563A23	CRISPR-Cas9 genome editing of 13563 cell line	This study

Table S1. List and origin of *v-abl* pro-B cell lines, Related to Figure 1

A

EXPMT 1	Cell line #	NI	1 Gy	2.5 Gy	5 Gy
WT	12095	4.3 (100%)	4.12 (95.8%)	3.42 (79.5%)	1.49 (34.7%)
	12096	4.4 (100%)	4.31 (98.0%)	3.43 (78.0%)	1.11 (25.2%)
<i>Paxx</i> ^{-/-}	P96B1	4.3 (100%)	4.11 (95.6%)	2.27 (52.8%)	0.7 (16.3%)
	P96B13	4.5 (100%)	4.0 (88.9%)	2.78 (61.8%)	0.79 (17.6%)
<i>Xlf</i> ^{-/-}	16488	3.6 (100%)	2.17 (60.3%)	0.84 (23.3%)	0.37 (10.3%)
	X95-3	4.0 (100%)	3.58 (89.5%)	1.98 (49.5%)	0.57 (14.3%)
<i>Paxx</i> ^{-/-} <i>Xlf</i> ^{-/-}	XP1	4.4 (100%)	1.8 (40.9%)	0.69 (15.7%)	0.38 (8.6%)
	XP6	4.7 (100%)	1.97 (41.9%)	0.76 (16.2%)	0.41 (8.7%)
<i>Xrcc4</i> ^{-/-}	Xr-95-21	3.8 (100%)	2.9 (76.3%)	0.81 (21.3%)	0.35 (9.2%)
	Xr-95-23	4.2 (100%)	3.79 (90.2%)	1.68 (40.0%)	0.51 (12.1%)

EXPMT 2	Cell line #	NI	1 Gy	2.5 Gy	5 Gy
WT	12095	4.8 (100%)	4.23 (88.1%)	3.47 (72.3%)	2.0 (41.7%)
	12096	4.28 (100%)	3.78 (88.3%)	2.82 (65.9%)	1.17 (27.3%)
<i>Paxx</i> ^{-/-}	P96B1	4.43 (100%)	3.4 (76.7%)	2.78 (62.8%)	0.87 (19.6%)
	P96B13	4.54 (100%)	4.2 (92.5%)	2.6 (57.3%)	1.0 (22.0%)
<i>Xlf</i> ^{-/-}	16488	3.83 (100%)	3.2 (83.6%)	1.65 (43.1%)	0.63 (16.4%)
	X95-3	4.55 (100%)	3.48 (76.5%)	2.06 (45.3%)	0.72 (15.8%)
<i>Paxx</i> ^{-/-} <i>Xlf</i> ^{-/-}	XP1	4.48 (100%)	1.52 (33.9%)	1.39 (31.0%)	0.51 (11.4%)
	XP6	4.86 (100%)	1.98 (40.7%)	1.2 (24.7%)	0.6 (12.3%)
<i>Xrcc4</i> ^{-/-}	Xr-95-21	4.29 (100%)	2.76 (64.3%)	1.29 (30.1%)	0.47 (11.0%)
	Xr-95-23	4.33 (100%)	3.62 (83.6%)	2.43 (56.1%)	1.0 (23.1%)

EXPMT 3	Cell line #	NI	1 Gy	2.5 Gy	5 Gy
WT	12095	4.28 (100%)	4.3 (100.5%)	3.7 (86.4%)	2.4 (56.1%)
	12096	4.32 (100%)	3.77 (87.3%)	3.43 (79.4%)	2.11 (48.8%)
<i>Paxx</i> ^{-/-}	P96B1	4.54 (100%)	3.8 (83.7%)	3.04 (67.0%)	1.68 (37.0%)
	P96B13	4.29 (100%)	3.91 (91.1%)	2.97 (69.2%)	1.34 (31.2%)
<i>Xlf</i> ^{-/-}	16488	4.28 (100%)	3.54 (82.7%)	2.82 (65.9%)	0.97 (22.7%)
	X95-3	4.3 (100%)	3.6 (83.7%)	2.53 (58.8%)	0.84 (19.5%)
<i>Paxx</i> ^{-/-} <i>Xlf</i> ^{-/-}	XP1	4.2 (100%)	2.73 (65.0%)	1.23 (29.3%)	0.62 (14.8%)
	XP6	4.36 (100%)	2.88 (66.1%)	0.86 (19.7%)	0.5 (11.5%)
<i>Xrcc4</i> ^{-/-}	Xr-95-21	4.68 (100%)	3.02 (64.5%)	1.11 (23.7%)	0.59 (12.6%)
	Xr-95-23	4.57 (100%)	3.49 (76.4%)	2.38 (52.1%)	1.09 (23.9%)

B

		1 Gy		2.5 Gy	
		p value	Significant	p value	Significant
WT	vs <i>Paxx</i> ^{-/-}	0.39393	no	0.00865	yes
	vs <i>Xlf</i> ^{-/-}	0.01515	yes	0.00639	yes
	vs <i>Paxx</i> ^{-/-} <i>Xlf</i> ^{-/-}	0.00216	yes	0.00216	yes
	vs <i>Xrcc4</i> ^{-/-}	0.01515	yes	0.00216	yes
<i>Paxx</i> ^{-/-}	vs <i>Xlf</i> ^{-/-}	0.07764	no	0.06493	no
	vs <i>Paxx</i> ^{-/-} <i>Xlf</i> ^{-/-}	0.00216	yes	0.00216	yes
	vs <i>Xrcc4</i> ^{-/-}	0.02597	yes	0.00432	yes
<i>Xlf</i> ^{-/-}	vs <i>Paxx</i> ^{-/-} <i>Xlf</i> ^{-/-}	0.00865	yes	0.01515	yes
	vs <i>Xrcc4</i> ^{-/-}	0.52110	no	0.30952	no
<i>Paxx</i> ^{-/-} <i>Xlf</i> ^{-/-}	vs <i>Xrcc4</i> ^{-/-}	0.02597	yes	0.09307	no

Table S2. Irradiation sensitivity assay of pro-B cell lines, Related to Figure 1

(A) Numbers indicate cell counts (10^6 cells/ml) after 3 days irradiation at 1Gy, 2.5Gy and 5Gy. Percentages of viable cells compared to non irradiated cells are indicated in brackets.

(B) Statistical analysis was performed at 1 and 2.5 Gy using Mann Whitney test.

A

EXPMT 1	WT			<i>Paxx</i> ^{-/-}			<i>Xif</i> ^{-/-}			<i>Paxx</i> ^{-/-} <i>Xif</i> ^{-/-}		
	12095			P96B1			X95-3			XP1		
	Nb of 53BP1 foci/nuclei	Nuclei Nb	Nuclei %	Nb of 53BP1 foci/nuclei	Nuclei Nb	Nuclei %	Nb of 53BP1 foci/nuclei	Nuclei Nb	Nuclei %	Nb of 53BP1 foci/nuclei	Nuclei Nb	Nuclei %
Cell line #1	0	3387	67.5	0	3167	63	0	1879	37.4	0	703	14.1
	1	1236	24.6	1	1663	33.1	1	2475	49.3	1	2784	55.9
	2	263	5.2	2	167	3.3	2	526	10.5	2	1209	24.3
	>2	130	2.6	>2	33	0.6	>2	144	2.8	>2	284	5.7
	TOTAL	5016	100	TOTAL	5030	100	TOTAL	5024	100	TOTAL	4980	100
Cell line #2	0	3204	63.8	0	2348	46.7	0	2885	56.7	0	721	14.4
	1	1488	29.6	1	2188	43.5	1	1727	33.9	1	3101	62
	2	248	4.9	2	400	8	2	360	7.1	2	994	19.9
	>2	81	1.5	>2	92	1.8	>2	117	2.2	>2	188	3.7
	TOTAL	5021	100	TOTAL	5028	100	TOTAL	5089	100	TOTAL	5004	100

EXPMT 2	WT			<i>Paxx</i> ^{-/-}			<i>Xif</i> ^{-/-}			<i>Paxx</i> ^{-/-} <i>Xif</i> ^{-/-}			<i>Xrcc4</i> ^{-/-}			<i>Ku80</i> ^{-/-}			<i>Rag2</i> ^{-/-}		
	12095			P96B1			X95-3			XP1			Xr-95-21			12071			129F-C1		
	Nb of 53BP1 foci/nuclei	Nuclei Nb	Nuclei %	Nb of 53BP1 foci/nuclei	Nuclei Nb	Nuclei %	Nb of 53BP1 foci/nuclei	Nuclei Nb	Nuclei %	Nb of 53BP1 foci/nuclei	Nuclei Nb	Nuclei %	Nb of 53BP1 foci/nuclei	Nuclei Nb	Nuclei %	Nb of 53BP1 foci/nuclei	Nuclei Nb	Nuclei %	Nb of 53BP1 foci/nuclei	Nuclei Nb	Nuclei %
Cell line #1	0	3642	72.3	0	3407	67.9	0	3028	64.3	0	1373	27.4	0	1562	31.1	0	1703	33.6	0	3703	83
	1	958	19	1	1328	26.5	1	1292	27.4	1	2485	49.5	1	2394	47.6	1	2485	49	1	482	10.8
	2	292	5.8	2	200	4	2	292	6.2	2	937	18.7	2	864	17.2	2	716	14.1	2	166	3.7
	>2	148	2.9	>2	80	1.5	>2	98	2.1	>2	221	4.5	>2	207	4.1	>2	165	3.2	>2	109	2.4
	TOTAL	5004	100	TOTAL	5015	100	TOTAL	4710	100	TOTAL	5016	100	TOTAL	5027	100	TOTAL	5069	100	TOTAL	4460	100
Cell line #2	0	3124	74.1	0	2819	61.5	0	3161	63.2	0	1495	29.8	0	1592	31.5						
	1	926	22	1	1204	26.3	1	1568	31.3	1	2665	53	1	2533	50.1						
	2	132	3.1	2	330	7.2	2	237	4.7	2	700	13.9	2	779	15.4						
	>2	36	0.8	>2	232	5	>2	39	0.7	>2	164	3.2	>2	152	3						
	TOTAL	4218	100	TOTAL	4585	100	TOTAL	5005	100	TOTAL	5024	100	TOTAL	5056	100						

EXPMT 3	WT			<i>Paxx</i> ^{-/-}			<i>Xif</i> ^{-/-}			<i>Paxx</i> ^{-/-} <i>Xif</i> ^{-/-}			<i>Xrcc4</i> ^{-/-}			<i>Ku80</i> ^{-/-}			<i>Rag2</i> ^{-/-}		
	12095			P96B1			X95-3			XP1			Xr-95-21			12071			129F-C1		
	Nb of 53BP1 foci/nuclei	Nuclei Nb	Nuclei %	Nb of 53BP1 foci/nuclei	Nuclei Nb	Nuclei %	Nb of 53BP1 foci/nuclei	Nuclei Nb	Nuclei %	Nb of 53BP1 foci/nuclei	Nuclei Nb	Nuclei %	Nb of 53BP1 foci/nuclei	Nuclei Nb	Nuclei %	Nb of 53BP1 foci/nuclei	Nuclei Nb	Nuclei %	Nb of 53BP1 foci/nuclei	Nuclei Nb	Nuclei %
Cell line #1	0	3389	67.7	0	3127	62.1	0	2146	42.8	0	946	18.9	0	1025	20.5	0	1891	37.7	0	4076	80.8
	1	1352	27	1	1686	33.5	1	2291	45.7	1	2672	53.3	1	2526	50.5	1	2217	44.3	1	720	14.3
	2	205	4.1	2	193	3.8	2	466	9.3	2	1163	23.2	2	1130	22.6	2	739	14.8	2	169	3.4
	>2	58	1.2	>2	29	0.6	>2	106	2.1	>2	235	4.7	>2	325	6.5	>2	163	3.3	>2	79	1.5
	TOTAL	5004	100	TOTAL	5035	100	TOTAL	5009	100	TOTAL	5016	100	TOTAL	5006	100	TOTAL	5010	100	TOTAL	5044	100
Cell line #2	0	3381	67.6	0	2106	41.9	0	2787	55.5	0	786	15.6	0	1156	23.1						
	1	1447	28.9	1	2354	46.8	1	1883	37.5	1	3073	61	1	2597	51.8						
	2	138	2.8	2	508	10.1	2	306	6.1	2	1022	20.3	2	941	18.8						
	>2	35	0.6	>2	59	1.1	>2	45	0.9	>2	154	3.1	>2	315	6.3						
	TOTAL	5001	100	TOTAL	5027	100	TOTAL	5021	100	TOTAL	5035	100	TOTAL	5009	100						

B

WT			<i>Paxx</i> ^{-/-}			<i>Xif</i> ^{-/-}			<i>Paxx</i> ^{-/-} <i>Xif</i> ^{-/-}			<i>Xrcc4</i> ^{-/-}			<i>Ku80</i> ^{-/-}			<i>Rag2</i> ^{-/-}		
Nb of 53BP1 foci/nuclei	Nuclei Nb	Nuclei %	Nb of 53BP1 foci/nuclei	Nuclei Nb	Nuclei %	Nb of 53BP1 foci/nuclei	Nuclei Nb	Nuclei %	Nb of 53BP1 foci/nuclei	Nuclei Nb	Nuclei %	Nb of 53BP1 foci/nuclei	Nuclei Nb	Nuclei %	Nb of 53BP1 foci/nuclei	Nuclei Nb	Nuclei %	Nb of 53BP1 foci/nuclei	Nuclei Nb	Nuclei %
0	20127	68.8	0	16974	57.2	0	15886	53.3	0	6024	20.0	0	5335	26.6	0	3594	35.7	0	7779	81.9
1	7407	25.2	1	10423	35.0	1	11236	37.5	1	16780	55.8	1	10050	50.0	1	4702	46.7	1	1202	12.6
2	1278	4.3	2	1798	6.1	2	2187	7.3	2	6025	20.1	2	3714	18.5	2	1455	14.5	2	335	3.6
>2	488	1.6	>2	525	1.8	>2	549	1.8	>2	1246	4.2	>2	999	5.0	>2	328	3.3	>2	188	2.0
Total nuclei	29300	100	TOTAL	29720	100	TOTAL	29858	100	TOTAL	30075	100	TOTAL	20098	100	TOTAL	10079	100	TOTAL	9504	100

Table S3. *Paxx*^{-/-} *Xif*^{-/-} *v-abl* pro-B cell harbor increased 53BP1 DDR foci after RAG induction, Related to Figure 2

(A) Table indicates the numbers and percentages of *v-abl* pro-B cells harboring 0, 1, 2 or >2 53BP1 foci 65h after ABLki treatment. Three independent experiments are shown.

(B) Table indicates total nuclei numbers and mean percentages of the experiments detailed in table A.

WT

Sequence #	5' SE	MH	N	3' SE	clones/total
	GGTTTTGTCCAGTCTGTAGCACTGTG			CACAGTGGTAGTACTCCACTGTCTGGCTGTACAAAAACC	
1	GGTTTTGTCCAGTCTGTAGCACTGTG			CACAGTGGTAGTACTCCACTGTCTGGCTGTACAAAAACC	38/42
2	GGTTTTGTCCAGTCTGTAGCACTGTG		GG	CACAGTGGTAGTACTCCACTGTCTGGCTGTACAAAAACC	1/42
3	GGTTTTGTCCAGTCTGTAGCACTGTG		AG	CACAGTGGTAGTACTCCACTGTCTGGCTGTACAAAAACC	1/42
4	GGTTTTGTCCAGTCTGTAGCACTGTG		AC	CACAGTGGTAGTACTCCACTGTCTGGCTGTACAAAAACC	1/42
5	GGTTTTGTCCAGTCTGTAGCACTGTG		CC	CACAGTGGTAGTACTCCACTGTCTGGCTGTACAAAAACC	1/42

Paxx^{-/-}

Sequence #	5' SE	MH	N	3' SE	clones/total
	GGTTTTGTCCAGTCTGTAGCACTGTG			CACAGTGGTAGTACTCCACTGTCTGGCTGTACAAAAACC	
1	GGTTTTGTCCAGTCTGTAGCACTGTG			CACAGTGGTAGTACTCCACTGTCTGGCTGTACAAAAACC	83/89
2	GGTTTTGTCCAGTCTGTAGCACTGTG		AG	CACAGTGGTAGTACTCCACTGTCTGGCTGTACAAAAACC	1/89
3	GGTTTTGTCCAGTCTGTAGCACTGTG		CC	CACAGTGGTAGTACTCCACTGTCTGGCTGTACAAAAACC	1/89
4	GGTTTTGTCCAGTCTGTAGCACTGTG		GGGAT	CACAGTGGTAGTACTCCACTGTCTGGCTGTACAAAAACC	1/89
5	GGTTTTGTCCAGTCTGTAGCACTG			CACAGTGGTAGTACTCCACTGTCTGGCTGTACAAAAACC	1/89
6	GGTTTTGTCCAGTCTGTAGCACTG			CAGTGGTAGTACTCCACTGTCTGGCTGTACAAAAACC	1/89
7	GGTTTTGTCCAGTCTGTAGCACTGTG		409 bp	CCACGTGTATAAGAT (-384) ATAAGAT	1/89

Xlf^{-/-}

Sequence #	5' SE	MH	N	3' SE	clones/total
	GGTTTTGTCCAGTCTGTAGCACTGTG			CACAGTGGTAGTACTCCACTGTCTGGCTGTACAAAAACC	
1	GGTTTTGTCCAGTCTGTAGCACTGTG			CACAGTGGTAGTACTCCACTGTCTGGCTGTACAAAAACC	29/46
2	GGTTTTGTCCAGTCTGTAGCACTGTG		CC	CACAGTGGTAGTACTCCACTGTCTGGCTGTACAAAAACC	2/46
3	GGTTTTGTCCAGTCTGTAGCACTGT			CACAGTGGTAGTACTCCACTGTCTGGCTGTACAAAAACC	1/46
4	GGTTTTGTCCAGTCTGTAGCACTGT		C	CACAGTGGTAGTACTCCACTGTCTGGCTGTACAAAAACC	1/46
5	GGTTTTGTCCAGTCTGTAGCACTGTG		CG	CAGTGGTAGTACTCCACTGTCTGGCTGTACAAAAACC	1/46
6	GGTTTTGTCCAGTCTGTAGCACTG		CG	CACAGTGGTAGTACTCCACTGTCTGGCTGTACAAAAACC	1/46
7	GGTTTTGTCCAGTCTGTAGCACTG		CCC	CACAGTGGTAGTACTCCACTGTCTGGCTGTACAAAAACC	1/46
8	GGTTTTGTCCAGTCTGTAGCACTGTG			CAGTGGTAGTACTCCACTGTCTGGCTGTACAAAAACC	1/46
9	GGTTTTGTCCAGTCTGTAGCACTGT	G		TGGTAGTACTCCACTGTCTGGCTGTACAAAAACC	1/46
10	GGTTTTGTCCAGTCTGTAGCACTG		CG	AGTGGTAGTACTCCACTGTCTGGCTGTACAAAAACC	1/46
11	GGTTTTGTCCAGTCTGTAGCACTG		AG	GTGGTAGTACTCCACTGTCTGGCTGTACAAAAACC	1/46
12	GGTTTTGTCCAGTCTGTAGCAC			CAGTGGTAGTACTCCACTGTCTGGCTGTACAAAAACC	1/46
13	GGTTTTGTCCAGTCTGTAG	CAC		AGTGGTAGTACTCCACTGTCTGGCTGTACAAAAACC	3/46
14	GGTTTTGTCCAGTCTGTAGCACT	GT		AGTACTCCACTGTCTGGCTGTACAAAAACC	1/46
15	GGTTTTG			CACAGTGGTAGTACTCCACTGTCTGGCTGTACAAAAACC	1/46

Paxx^{-/-} *Xlf*^{-/-}

Sequence #	5' SE	MH	N	3' SE	clones/total
	GGTTTTGTCCAGTCTGTAGCACTGTG			CACAGTGGTAGTACTCCACTGTCTGGCTGTACAAAAACC	
1	GGTTTTGTCCAGTCTGTAGCACTGTG			CACAGTGGTAGTACTCCACTGTCTGGCTGTACAAAAACC	14/88
2	GGTTTTGTCCAGTCTGTAGCACTGTG		804	CACAGTGGTAGTACTCCACTGTCTGGCTGTACAAAAACC	1/88
3	GGTTTTGTCCAGTCTGTAGCACTG			CACAGTGGTAGTACTCCACTGTCTGGCTGTACAAAAACC	1/88
4	GGTTTTGTCCAGTCTGTAGCACTG			CAGTGGTAGTACTCCACTGTCTGGCTGTACAAAAACC	1/88
5	GGTTTTGTCCAGTCTGTAGCA	C		ACAGTGGTAGTACTCCACTGTCTGGCTGTACAAAAACC	1/88
6	GGTTTTGTCCAGTCTGTAGCACTGTG			GGTAGTACTCCACTGTCTGGCTGTACAAAAACC	1/88
7	GGTTTTGTCCAGTCTGTAGCACT		A	AGTGGTAGTACTCCACTGTCTGGCTGTACAAAAACC	1/88
8	GGTTTTGTCCAGTCTGTAGCACT			AGTGGTAGTACTCCACTGTCTGGCTGTACAAAAACC	1/88
9	GGTTTTGTCCAGTCTGTAGCA	C		AGTGGTAGTACTCCACTGTCTGGCTGTACAAAAACC	2/88
10	GGTTTTGTCCAGTCTGTAG	CAC		AGTGGTAGTACTCCACTGTCTGGCTGTACAAAAACC	12/88
11	GGTTTTGTCCAGTCTGTAGCACT	GTG		GTAGTACTCCACTGTCTGGCTGTACAAAAACC	2/88
12	GGTTTTGTCCAGTCTGTAGCAC			GTGGTAGTACTCCACTGTCTGGCTGTACAAAAACC	1/88
13	GGTTTTGTCCAGTCTGTAGCACTG			GGTAGTACTCCACTGTCTGGCTGTACAAAAACC	2/88
14	GGTTTTGTCCAGTCTGTAG	CA		GTGGTAGTACTCCACTGTCTGGCTGTACAAAAACC	6/88
15	GGTTTTGTCCAGTCTGTAGCACT	GT		AGTACTCCACTGTCTGGCTGTACAAAAACC	1/88
16	GGTTTTGTCCAGTCTG		C	CACAGTGGTAGTACTCCACTGTCTGGCTGTACAAAAACC	1/88
17	GGTTTTGTCCAGTCTGTAG		A	TGGTAGTACTCCACTGTCTGGCTGTACAAAAACC	1/88
18	GGTTTTGTCCAGTCT	GT		GGTAGTACTCCACTGTCTGGCTGTACAAAAACC	1/88
19	GGTTTTGTCCAGTCTG			GGTAGTACTCCACTGTCTGGCTGTACAAAAACC	2/88
20	GGTTTTGTCCAGTCTG		C	GGTAGTACTCCACTGTCTGGCTGTACAAAAACC	1/88
21	GGTTTTGTCCAG		G	AGTGGTAGTACTCCACTGTCTGGCTGTACAAAAACC	2/88
22	GGTTTTGTCCAGTCT	GTAG		TACTCCACTGTCTGGCTGTACAAAAACC	4/88
23	GGTTTTGTT	C		ACAGTGGTAGTACTCCACTGTCTGGCTGTACAAAAACC	1/88
24	GGTTTTGTT	CAGT		GGTAGTACTCCACTGTCTGGCTGTACAAAAGACC	2/88
25	GGTTTTGTCCAGTCTGTAGCACTG			CTGTCTGGCTGTACAAAAACC	1/88
26	GGTTTTGTCCAGTCT	GTA		CTCCACTGTCTGGCTGTACAAAAACC	1/88
27	GGTTTTGTCCAGTCTGTAG	CACTGT		CTGGCTGTACAAAAACC	1/88
28	GGTTTTGTCCAGTCTG		G	TCCACTGTCTGGCTGTACAAAAACC	1/88
29	GGTTTTGTCCAGTCTGTAG	C		TGTCTGGCTGTACAAAAACC	2/88
30	GGTTTTGTT	C		TCCACTGTCTGGCTGTACAAAAACC	1/88
31	GGTTTTGTCCAGTCTGTA	G		GCTGTACAAAAACC	1/88
32	GGTTTTGTCCAG	T		GTCTGGCTGTACAAAAACC	1/88
33	G	G		GTAGTACTCCACTGTCTGGCTGTACAAAAACC	1/88
34	GG			GTA TCCACTGTCTGGCTGTACAAAAACC	4/88
35	GGTTTTGTT	C		TGGCTGTACAAAAACC	2/88
36	GGTTTTGT	TC		TGGCTGTACAAAAACC	1/88
37	GGTTTTGTCCAGTCTGTA	GCAC		(-45) GCACCCGGGTA CCGGGTA	1/88
38	<i>GGATCTCGCGG</i> GGATCT (-53)		T	TGTCTGGCTGTACAAAAACC	1/88
39	<i>GCCGACCCCGG</i> GCCGACC (-87)		162 bp	CACAGTGGTAGTACTCCACTGTCTGGCTGTACAAAAACC	1/88
40	GGTTTTGTCCAGTCTGTAGCACTGTG		221 bp	(-199) CCTGTCTTCTGA TTCITGA	1/88
41	GGTTTTGTCCAGTCTGTAGCACTG	TG		(-327) CCTTTGCAGGCA CAGGCA	1/88
42	GGTTTTGTCCAGTCTGTAGCACTGTG		192 bp	(-347) CACTGGCGACA CTGGCGACA	1/88
43	GGTTTTGTCCAGTCTGTAGCACTG		223 bp	(-397) ACCTGCAAAGGC CTGCAAAGGC	1/88
44	<i>AGACCTCTGGCGG</i> AGACCT (-298)	CTGGCG		(-347) CCTGGCGACAGG ACAGG	1/88
45	<i>GTCCGCCGACCC</i> GTCCGCC (-216)			(-440) GATAGTTGTGGA TTGTGGA	1/88

Table S4. Signal Joints sequences from WT:DEL^{SJ}, *Paxx*^{-/-}:DEL^{SJ}, *Xlf*^{-/-}:DEL^{SJ} and *Paxx*^{-/-} *Xlf*^{-/-} DEL^{SJ} *v-abl* pro-B cells, Related to Figure 4

Reference sequences for 5' and 3' signal ends generated from pMX-DEL^{SJ} substrate are indicated on top. Microhomologies (MH) and N-nucleotides additions are indicated. For sequences with additions greater than 5 nucleotides, the numbers of additional bases pairs are indicated instead. When signal ends are resected further than the reference sequence, the numbers of resected nucleotides are shown in brackets along with the reference sequence flanking the resected end in italics. Frequency of unique sequence is indicated (last column). *Paxx*^{-/-} *Xlf*^{-/-} sequences were obtained from two independent cell lines (XP1, XP6).